UNIVERSITAT DE BARCELONA

Active turbulence and active shell models for microswimmer suspensions

Toni Gascó Patiño

UNIVERSITAT DE BARCELONA

DOCTORAL THESIS

Active turbulence and active shell models for microswimmer suspensions

Author: **Toni Gascó Patiño**

Directors: **Dr. Ignasi Pagonabarraga Mora**
Dr. Andrea Scagliarini

UNIVERSITAT DE BARCELONA

Active turbulence and active shell models for microswimmer suspensions

Programa de doctorat en Física

Au t or: **Toni Gascó Patiño**

Directors: **Dr. Ignasi Pagonabarraga Mora**
Dr. Andrea Scagliarini

Tutor: **Dr. Giancarlo Franzese**

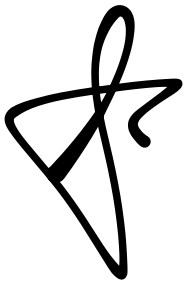

Aquesta tesi doctoral s'ha realitzat a la Facultat de Física

Barcelona 2023

DOCTORAL THESIS REPORT TO APPLY FOR THE DOCTORAL DEGREE
FOR THE UNIVERSITY OF BARCELONA

Active turbulence and active shell models for microswimmer suspensions

Author: Toni Gascó Patiño
Director: Dr. Ignasi Pagonabarraga Mora
Co-director: Dr. Andrea Scagliarini
Management: Dr. Giancarlo Franzese
Doctoral program coordinator: Dr. Assumpta Parreño

Faculty of Physics

Line of research: Condensed matter physics.
Thursday 19th October, 2023

To my family and Spotify
because without their soundtrack
it would not have been possible.

Abstract

The goal of this thesis is to study the collective behavior of active matter by numerical simulations, specifically microswimmers dynamics in a semi-dilute suspension. We want to explore the capabilities of basic physical ingredients to generate emergent structures on scales much larger than those of individual agents. The aim is to improve the understanding of the phenomenon of active turbulence as a paradigmatic and fascinating example of self-organized motion at large scales in active matter.

Some massive hydrodynamic simulations of suspensions of resolved model microswimmers, using an open source code based in Lattice-Boltzmann Methods (LBM), are presented. We mesure the kinetic energy spectrum studying the energy flows through the different scales in which the system breaks down and we also calculate the mean squared displacement and polar order of the system, showing that there are significant differences in the behavior of the so-called pushers and pullers.

Furthermore, we propose a dynamical deterministic model for active turbulence, inspired to shell models for classical turbulence. Several computational simulations have been performed using the implementation of this model in a specific code, whose numerical and analytical study confirms the spectrum power-law predicted by theory and observed in the LBM simulations.

Acknowledgements

I would like to thank my director, Dr. Ignasi Pagonabarraga, for his explanations and his guide throughout the process of creating this doctoral thesis.
I want to thank Dr. Andrea Scagliarini as co-director for his great help in carrying out this thesis at a technical and theoretical level.
And I also want to thank Dr. Francisco Alarcón for his collaboration in the final part of the research.

Toni Gascó
Thursday 19th October, 2023

When I meet God I will ask him two questions:
Why relativity? And why the turbulence?
I'm sure he will get the answer of the first one.

Werner Heissenberg

Outline of the Thesis

This doctoral thesis deals with the study of the collective behavior of active particles using computacional simulations of semi-dilute solutions of microswimmers. Results are obtained for the polar order parameter, the diffusion and the energy spectrum among others as a function of the concentration and the degree of orientation of the particles. Our main interest is to improve the understanding of the relation between energy flows through the scales of the system and the characteristic collective movements that occur spontaneously and that can be easily recognized in a wide range of situations in different fields (banks of fish, flocks of birds, bacterial cultures, polymer solutions, etc) into a regime that we can refer to as soft active turbulence.

Shell models are deterministic dynamical systems that reduce the complexity of the full field equations, though retaining some of their essential features. Originally introduced as a proxy of the Navier-Stokes equations, and therefore characterized by a quadratic nonlinearity and the same inviscid invariants (energy and helicity). Since *GOY-model* is the original shell model that reproduces aspects of inertial turbulence through a modeling of the system as a sort of Fourier amplitudes of velocity fluctuations over a length scale with associated wavenumber k_n [22-25], our main aim is to propose a new generalized shell model that can capture some basic properties of the active turbulence dynamics but not trajectories or any other geometric aspect. In the bibliography one can find an improved version of *GOY* called *SABRA-model* [34][36][37] and other variations of the original idea [28][29], although all performed the interaction of shells on a single field. For this reason, our goal is to perform simulations with a generalized *SABRA-model* developed from the interaction and self-action of two fields. The nature of these fields

as well as the form of the model equations places the theoretical framework in the field of active matter and this is the reason why we refer to the proposed model as *SabrActive-model*. In this sense, several simulations have been carried out with a specific code to quantify the impact of the variations of the main parameters of the model: the concentration and orientation of the active particles (squirmers).
On the other hand, with the intention of knowing better the collective behavior of the active matter and, to a certain extent, to validate the results obtained with the shell model, several computational simulations have been carried out with Ludwig code, which is an open source code based on the Lattice-Boltzmann method for simulating complex three-dimensional fluids. With this code it is possible to configure multiple models with different values of free energy and other parameters. The program allows for the creation of periodic boundary conditions, interaction between suspended colloids, liquid crystals and binary fluids.
Therefore, there are two very well differentiated parts in this work, which is structured in six chapters.

Chapter 1 is a topic introduction that defines what are the active systems and the consequence to have a set of active particles. In this chapter, we also explain the theoretical framework.

Chapter 2 explains the numerical methodology that we use to simulate the fluid that interact with active particles. A full review of the Lattice-Boltzmann method is depicted here. Some specific aspects of the code that we have used to carry out the simulations, whose results are presented in the following two chapters, are also commented on.

Chapter 3 shows some results of massive hydrodynamic simulations of suspensions of resolved model microswimmers using the Lattice- Boltzmann method. Parametric variations of the concentration and orientation of the particles are made. From the obtained results we study the mean squared displacement and the polar order, concluding that in a certain range of the parameter space a clear increase in diffusion linked to a spontaneous increase in the polar order of the system can be observed. This chapter also studies how collectively affects whether the self-driven

displacement of the active particles is carried out in the direction of the individual orientation or in the opposite direction (puller or pusher particles).

In Chapter 4 the same simulation results from the previous chapter are used to calculate the mean and normalized energy spectrum. In Fourier space the system breaks down into a superposition of modes that are interpreted as different scales. The energy flows towards the higher scales are defined as inverse cascade phenomena, and in the opposite direction we speak of direct cascade. We try to better understand the flow of energy through the scales by studying the local slope of the inertial zone of the spectra.

The second part of the thesis, the one that deals with shell models, is developed in Chapter 5. First, there is a brief introduction of the concepts that motivate the appearance of this type of models. The *GOY-model* and *SABRA-model* are described below as a basis from which to generalize towards models applicable to active matter. Starting from two vector fields, one of velocities and the other of individual orientations of the particles, a set of differential equations that include different terms with the interaction and self-action between the fields are proposed as generators of the system dynamics. The key of *SabrActive-model* is the function that relates different scales of both fields in a bound way, expressing them as modes in Fourier space. As such, it offers the possibility to investigate the chaotic dynamics and multiscale correlations of turbulence with obvious computational advantages. So *SabrActive-model* is described in this chapter at the structure, dynamics and parameter level. Various computational simulations are performed with this model implemented in a specific code. The processing and study of the results allows us to observe direct and inverse cascade phenomena in the energy spectrum demostrating that this model is a useful tool to generate in a simple way and help understand certain collective behaviors of the active matter.

Finally in Chapter 6 the conclusions and future directions of the research.

Contents

CHAPTER

1

Introduction

In this chapter, we give a general definition of *active matter* and *active particles*. We refer specifically about a type of particles that since they interact with the fluid to self-propel themselves, they are called *microswimmers*. We present below a selection of the theoretical background generated in the recent years for active matter focusing on those aspects on which they are based the set of equations that we used along the computational study through which we explore the capabilities of basic physical ingredients to generate emergent structures on scales much larger than those of individual agents.

1.1 Active Matter

Forms of self-organized motion show in nature how disparate systems can exhibit a number of common phenomena from mesoscopic to large scale. Several researchers have been working to understand the fundamental mechanisms that generate the collectivity between particles, like clustering, polar order or phase separation [14-18]. The term *active* first appeared in a paper by Ramaswamy and Simha (2006) as the appellation of a fledgling research field that has been rapidly expanding since then. Active systems can be defined as materials which are made of many interacting units, where each unit consume energy and generate motion.

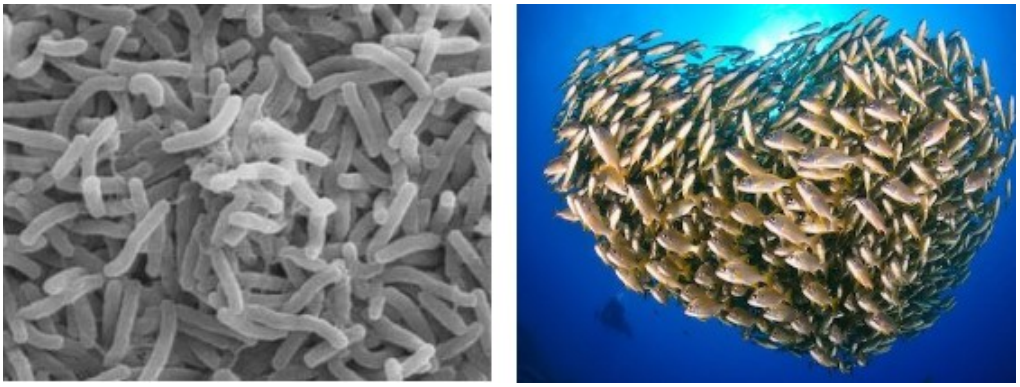

Figure 1.1: *Bacteria suspensions and schools of fish can be considered examples of active matter with common dynamic properties.*

Figure 1.1 shows two representative examples of this behavior, applicable to many more living beings, objects and systems of all kinds.
There are two essential classifications of the active matter. The first distinguishes between living organisms and artificial objects. The second classification is based on the relationship between the active particle and the fluid medium in which it is embedded. If there is a significant exchange of energy with the environment, maintaining conservation of momentum, the system is called wet. If, on the other hand, the fluid is merely testimonial and the dynamics of the particles develop without significant interference from the medium, then the system is classified as dry. Note that the first classification (live-artificial) refers to the nature of the particles while the second (dry-wet) arises from the type of modeling. All these kinds of systems are intrinsically out of equilibrium.

Some aspects of the behavior of diluted microswimmer suspensions are reminiscent, on a visual level at least as we can see in FIG.1.2, of the behavior of fluids in a turbulent regime at low Reynolds numbers [1][3]. In both types of systems cooperation occurs spontaneously, and it is regulated with a relatively small set of parameters making mesoscopic structures emerge. So we could assume that a description based on scale overlap (and on the transfer of energy through them) can be useful to describe the collective dynamics that is generated in active turbulence systems. Although, in the case of *active turbulence*, self-driven movement of the par-

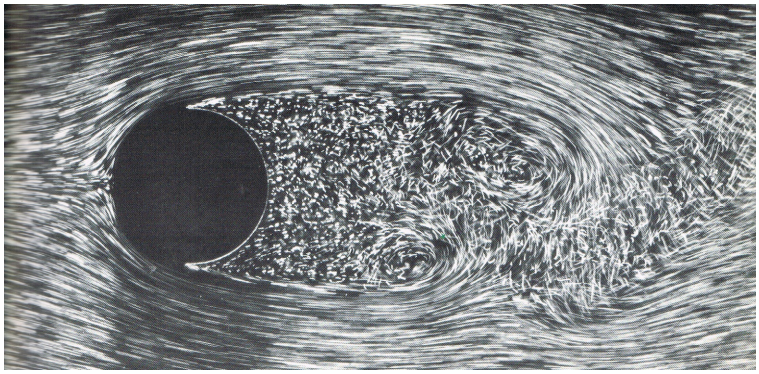

Figure 1.2: *Soft hydrodynamic turbulence shows visual aspects also present in the active matter. Image from ref [3]*

ticles replaces the mere inertia, increasing the complexity of the problem because a hybrid description of the active suspension is needed, which should combine the individual dynamics of particle with a kinetic model for the solvent. Power-law decays of kinetic energy spectra over unexpectedly wide ranges of wavenumbers have been identified as a signature of turbulent behaviour [13]. With the aim of analyzing multi-scale interactions and energy transfer, recent studies have focused on the spectral properties of continuum models [32][42] where the active fluid is described as an effective medium [11][14].

The range of applications in this field is very wide, in general active matter can be a good approach as long as activity is the innate feature of the particles that compose (and subcompose) the system:*"they are machines consisting of machines, and themselves parts of greater machines, which are already beyond the realm of mere matter"* [51]. The study of the equations proposed to model the active interaction between particles through computational simulations is frequent [9][10][41][57-61]. The level of calculation required is very high, since the simulation must include the maximum number of particles possible and the greatest range of interaction with the environment and the rest of the particles to represent the physical reality of the solution with guarantees. It could be said that supercomputers are the particle accelerators necessary to discover the emerging structures and mechanisms of active matter: the greater the power of the machine, the smaller

the range of interaction that can be observed with good resolution, so *Active Matter* could flourish only in this century.

What we can consider a particle is something difficult to specify, so that we can define active particle as each one of the components of a system considered active matter. Marchetti et al (2013) , in an all-round review co-authored by seven physicists [23], define active matter as *"composed of self-driven units, active particles, each capable of converting stored or ambient free energy into systematic movement"*, referring to Schweitzer (2003), who did not use this term, however. Note that in this definition, the interaction with the environment is included almost like an intrinsic feature. Several recent studies have led to significant theoretical advances in the understanding of these systems in continuous interaction with the environment that surrounds them [14-16][18-20] and they observe that collective movements or associations frequently take place. The collective behaviour of a lot of particles point to a correlation whose understanding is one of the main objectives of research.
It should be noted also that self-driven does not mean autonomous movement because it is always subject, at least to some degree, to external forces and/or collective interactions. Active particles are not free particles. We are not talking about shark but about plankton, about jellyfishes that propel themselves by absorbing and expelling the same water that drags them in the current. It could be a microbe wandering around looking for nutrients. It can be a bird or a fish, a part of a herd or shoal. It could be one person in a crowd [1].

Another feature of active particles is the presence of a dissipative range layer similar to convective structures in the oceans or atmosphere. Active gels, bacterial suspensions or liquid crystals are specific models of active particles. All this kind

[1] *Leonardo da Vinci* had called turbulence the process of the random movement of fluids for the first time in history from the Latin term *turba* meaning people. Turbulence therefore means movement of people. In fact, as can be seen in figure 1.3, Leonardo was already speculating with the idea of describing the turbulent regime as a superposition of different relatively simple curves, an idea that was perhaps already present in his time.

Figure 1.3: *Drawing of* Leonardo da Vinci *describing turbulence as a superposition.*

of particles can be called *microswimmers* because they extract energy from the environment to self-driven themselves. In this work we are going to be focused on one type of them, an artificial spherical microswimmers, called *squirmers*.
Live organisms commonly move by deforming their body, something inanimate particles cannot do, but *squirmers* can to swim even without external appendages, and even with no deformation, just by inducing tangential flow along the particle's surface [52][53]. In contrast to Brownian particles subject to thermal fluctuations, squirmers take up energy from the medium and convert it into net motion. Inertia plays no role in the motion of microscopic particles because self-velocity is great enough to consider Reynolds number close to unity.

Active particles are often assigned certain intrinsic characteristics, most commonly, their orientation. The orientation may determine their preferred direction of motion, e.g., with respect to gradients of an external field, or the character of their interactions, the tendency to align with their neighbours. The basic types of orientation are vector (denoting the direction) or nematic (implying an alignment without a definite direction, as in a vector without an arrow). Both kinds of orientation may or may not be qualified by their strength. The notion of intrinsic orientation comes from the physics of condensed matter [21], which engaged with directed interactions in solids and fluids long before studies of active matter came on the scene.

1.2 Field theory approach

Field theory used in this study is based on the interaction of the active particles with each other and with the environment in which they are located. This relation gives rise to correlated movements and mechanical stresses. The energy that takes the system out of equilibrium is, therefore, of local origin, each particle consumes and dissipates energy, and general patterns can be formed that are repeated in different experiments and simulations [14]. Hydrodynamic theories describe active suspensions in terms of the relevant field variables, namely the concentration field of bacteria, $c(x,t)$, the (incompressible) fluid velocity field, $u(x,t)$, and an order parameter quantifying the degree of local orientation.

In the simulations performed in this work, semi-dilute squirmer suspensions can develop alignment depending on the hydrodynamic signature, and this alignment has been measured by the polar order (vectorial) parameter, $P(x,t)$, representing the average, within a fluid element, of either the particle intrinsic swimming director, $P_i \propto \langle \widehat{e}_i \rangle$. The results are presented in Chapter 3.
Order paramenter can be also tensorial (nematic), $Q(x,t)$, using the dyadic product, $Q_{hk} \propto \langle \widehat{e}_h \widehat{e}_k \rangle$, to generate a tensor Q_{hk} which quantifies the degree of alignment of the axes of the particles of the system without distinction between head and foot.
Systems as those considered in this work can have nematic order without polar order [13-20] therefore, additionally to the polar order parameter, we also should consider the nematic order parameter, defined by the usual method [65] using the 3D nematic order

$$Q_{hk} = \frac{1}{N} \sum_{i=1}^{N} \left(\frac{3}{2} e_{ih}\left(t\right) e_{ik}\left(t\right) - \frac{\delta_{hk}}{2} \right) \tag{1.1}$$

where h and k are x, y, z and N the total amount of swimmers.

Active nematics theory is one of the most popular models in this field, although it is not the only one and it is not the most relevant in our work. In the shell model explained in chapter 5, a tensor field is not used, but a vector one.

CHAPTER

2

Numerical modeling

Lattice Boltzmann methods are a class of computational methods for simulating fluid dynamics. Instead of solving the Navier-Stokes equation, the discrete Boltzmann equation is used from the simulation of collision models of a Newtonian fluid. From a long and large enough iteration of a finite number of virtual particles that propagate and collide on a grid a microcosm of viscous fluid extrapolable to much larger masses is shown.
In first section we make an introduction; next we talk about Squirmer Model like a kind of self-propelled swimmer-model by simply inducing a tangential flow along the surface of the particle; third the Boltzman equation and its discretization is introduced as as a mathematical foundation; the Lattice Boltzmann method itself is explained also and, finally, we talk about the main characteristics of *Ludwig* (the code that we run in the simulations presented in chapters 3 and 4).

2.1 Introduction

When you want to model a large set of particles in hydrodynamic interaction, there are broadly two perspectives: describe the macroscopic behavior of the system or generate a series of rules that reproduce the interaction between the particles at a local (microscopic) level.

On a macroscopic scale, partial differential equations (PDE) like Navier-Stokes equation are used. Since these kind of equations are difficult to solve analytically due to non-linearity, complicated geometry and boundary conditions. A lot of numerical schemes such as finite difference method (FDM), finite volume method (FVM), finite element method (FEM) or spectral element method (SEM) are used to convert the PDE to a system of algebraic equations. These macroscopic methodology is based on the discretization of the PDE. However, we can lose details of the dynamic of the mesoscopic elements.
Another approach to the problem is to consider a microscopic scale where the motion of all the particles of the system can be simulate. The fact of the large disparity between the time-length scales of the solvent and the mesoscopic components make technically impossible to simulate complex fluids. To close the gap between macro-scale and micro-scale, coarse-grained models have been developed. These methods reduce the degrees of freedom of the solvent but capture the collective modes of the fluid. For example, in Brownian Dynamics the solvent is represented implicitly by random forces and frictional terms (it is a simplified version of Langevin dynamics where particle inertia is neglected). Lattice Boltzmann Method is another exemple, it is based on microscopic models and mesoscopic kinetic equations. The fundamental idea of the LBM is to construct simplified kinetic models that incorporate the essential physics of microscopic processes so that the macroscopic averaged properties obey the desired macroscopic equations [58]

LBM originated from cell automaton-based models with the goal of eliminating statistical noise by replacing the Boolean particle with the average motion of numerous particles in the same direction through the so-called probability density function. Discrete collisions are replaced by a continuous function called the collision operator. LBM places the fluid at a mesoscopic level, between the microscopic and the macroscopic level, trying to ensure that the collective dynamic recovers as it moves to the continuum. Even though the LBM is based on a particle picture, its principal focus is the averaged macroscopic behaviour. The kinetic equation provides many of the advantages of molecular dynamics, including clear physical pictures, easy implementation of boundary conditions, and fully parallel algorithms. Because of the availability of very fast and massively parallel machines, there is a

current trend to use codes that can exploit the intrinsic features of parallelism. The LBM fulfills these requirements in a straightforward manner [58].

2.2 Boltzmann Equation

To investigate fluxes in a dilute solution, it would be necessary to describe the dynamics of large numbers of particles, but it is clearly impossible to a tackle the displacement of each individual particle. However, when we focus on the meso and macro scales, the description of the motion of each individual particle is no longer necessary because macroscopic fields of interest [FT], such as e.g. densities, velocities, temperature, etc., can be calculated through hydrodynamic quantities given by local averages over numerous molecules.

The kinetic theory of gasses describes exactly how to perform this averaging, as well as how the hydrodynamic quantities evolve in time, via the introduction of the probability distribution function $f(\mathbf{x}, \mathbf{v}, t)$, a function of the position $\mathbf{x}$, velocity $\mathbf{v}$ and time t, giving the probability of finding a molecule close to the position $\mathbf{x}$, at time t, and with a velocity close to $\mathbf{v}$. From this mesoscopic quantity, f, it is then possible to define how hydrodynamics fields such as the density ρ and the fluid velocity $\mathbf{u}$ can be derived as moments of $f(\mathbf{x}, \mathbf{v}, t)$. In particular, the density of the fluid can be computed by first looking at the probability of finding a particle in a given position $\mathbf{x}$ with any velocity $\mathbf{v}$ and thus by finally integrating over the full velocity space:

$$\rho(\mathbf{x}, t) = \int f(\mathbf{x}, \mathbf{v}, t) d\mathbf{v} \tag{2.1}$$

Similarly the macroscopic flow momentum is computed as:

$$\rho(\mathbf{x}, t)\mathbf{u}(\mathbf{x}, t) = \int f(\mathbf{x}, \mathbf{v}, t)\mathbf{v} d\mathbf{v} \tag{2.2}$$

And also the temperature, T, and the heat flux, q, could be calculated as:

$$T = \frac{1}{k_B \rho} \int (\mathbf{v} - \mathbf{u})^2 f(\mathbf{x}, \mathbf{v}, t) d\mathbf{v} \tag{2.3}$$

$$q = \frac{1}{2} \int (\mathbf{v} - \mathbf{u})^3 f(\mathbf{x}, \mathbf{v}, t) d\mathbf{v} \tag{2.4}$$

To describe the evolution of the distribution function, $f(\mathbf{x}, \mathbf{v}, t)$, the Bolzmann Equation (BE) can be used

$$\partial_t f + \mathbf{v}\nabla_x f + \mathbf{a}\nabla_v f = \Omega(f) \tag{2.5}$$

In this equation, we can find a time evolution operator, $\partial_t f$, a transport term, $\mathbf{v}\nabla_x f$, a forcing term modeling the external force contribution ($\mathbf{a} = \frac{\mathbf{F}}{m}$), $\mathbf{a}\nabla_v f$ and, on the other hand, the collision operator, $\Omega(f)$ describing all the interacions occuring between the particles.

This equation cannot be solved until the collision operator is properly defined. The collision operator can be complicated to describe as it depends upon many parameters including the intermolecular force occurring between particles. One way to simplify the treatment of the collision operator is the usually applied BGK (Bhatnagar - Gross - Krook) approximation. Such BGK collision operator corresponds to a first order Taylor expansion with respect to equilibrium, and it can be expressed in the form of

$$\Omega = -\frac{1}{\tau}(f - f^{eq}) \tag{2.6}$$

τ represents the relaxation time, while f^{eq} is the function describing the local equilibrium. In the BGK collision operator, the local equilibrium is assumed to be the usual Maxwell-Boltzman equilibrium which is given, per unit mass, by a Gaussian distributed ($\sim \mathcal{N}(\mathbf{u}, T)$) function

$$f^{eq}(\mathbf{x}, \mathbf{v}, t) = \frac{\rho(\mathbf{x}, t)}{(2\pi k_B T)^{3/2}} e^{\frac{-(\mathbf{v}(\mathbf{x},t)-\mathbf{u}(\mathbf{x},t))^2}{2k_B T}} \tag{2.7}$$

Collisions must conserve the quantities of mass, momentum and energy, as initially assumed for the probability distribution function. The conservation constrains as moments of the collision operator, are expressed as:

mass conservation

$$\int \Omega f^{eq} d^3\mathbf{v} = 0 \tag{2.8}$$

conservation of the moment

$$\int \Omega f^{eq} \mathbf{v} d^3\mathbf{v} = 0 \tag{2.9}$$

energy conservation

$$\int \Omega f^{eq} \mathbf{v}^2 d^3\mathbf{v} = 0 \tag{2.10}$$

2.3 Lattice-Boltzmann-Method

As FIG.2.1 and FIG.2.2 show, the Lattice-Boltzmann model (LBM) simulates the Boltzmann equation with linearized collisions on a lattice . Both the changes in position and velocity are discretized. It can be shown that, at sufficiently large length and time scales, LBM simulates the dynamics of nearly incompressible viscous flows. For the simplest case of a one-component fluid, it describes the evolution of a discrete set of particle densities on the sites (or nodes) of a lattice:

$$f_i(\mathbf{r} + \mathbf{c_i}, t+1) - f_i(\mathbf{r} + \mathbf{c_i}, t) = -\omega \left(f_i^{eq}(\mathbf{r}, t) - f_i(\mathbf{r}, t)\right) \tag{2.11}$$

The quantity $f_i(\mathbf{r}, t)$ is the density of particles with velocity $\mathbf{c_i}$ resident at node $\mathbf{r}$ at time t. This particle density will, in unit time increment, be convected (or propagate) to a neighboring site $\mathbf{r}+ \mathbf{c_i}$. Here $\mathbf{c_i}$ is a lattice vector, or link vector, and the model is characterized by a finite set of these velocities. The quantity $f_i^{eq}(\mathbf{r}, t)$ is the equilibrium distribution of $f_i(\mathbf{r}, t)$, and is one of the key ingredients of the model. It characterizes the type of fluid that the code that we use to perform the experimental results, *Ludwig*, will simulate, and determines the equilibrium properties of such a fluid. The right hand side of equation describes a mixing of the different particle densities, or collision: the f_i distribution relaxes towards f_i^{eq} at a rate determined by ω, the relaxation parameter, which is related to the dynamic viscosity of the fluid, and gives us control of its dynamics: $\eta = (\frac{2\omega^{-1}-1}{6})$

Various types of grids, triangular or cubic, can be used in the discrete distribution function to apply LBM. The most common way to classify each method is the form D_nQ_m. D_n represents the n dimensions and Q_m represents the m possible directions of motion at each step through the virtual particle, that is, m different velocities. For example, D_3Q_{19} is a three-dimensional *Lattice Boltzmann* model on a cubic grid where particles can rest or change position. Each node has the shape of a lattice crystal and can pass particles to any of the eight adjacent nodes located in

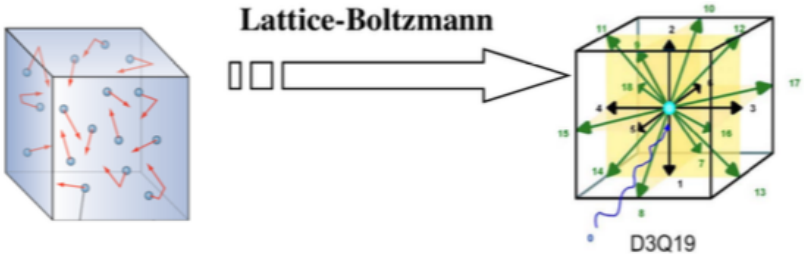

Figure 2.1: Discretization of the movement of the particles in the grid with the LBM, describing the evolution of a discrete set of particle densities on the sites (or nodes) of a lattice.

Figure 2.2: Graphic representation of a 3D grid with 19 possible changes of position. Each node has the shape can pass particles to any of the eight adjacent nodes located in the same plane, with the ten nodes located in the immediately upper or lower plane or can stay in the same node.

the same plane of the lattice, with the five nodes located in the immediately upper plane, with the five nodes located in the immediately lower plane and with the same node (rest).

2.4 Interaction between moving particles and fluid flow

In the particle transport problems concerned, the solid particles are mainly driven by the hydrodynamic forces exerted by the fluid, and the body forces if considered. In the context of LB methodology, fluid particles impact the boundary of the solid particle, and they exchange momentum to alter their motion. It is important to correctly model the interactions between fluid and solid particles so as to capture the essential physical behaviour of the problem under consideration. This requires a physically correct "no-slip" boundary condition to impose at the interface between the fluid and the particle, i.e. the fluid adjacent to the particle surface should have the velocity identical to the particle surface. For stationary particles the bounce-back rule (which means a reflection in the same direction but in different sense) can be imposed to accomplish

$$f_{-i}(\mathbf{x}, t+1) = f_i(\mathbf{x}, t) \tag{2.12}$$

The first step to model fluid and solid particle interaction is to represent the particle by lattice nodes. In a lattice discretization of a spherical particle there will be nodes interior and exterior to the particle , i.e., solid and fluid nodes. These nodes are further classified into three categories:

- Fluid boundary node. A fluid node connected at least with one solid node
- Solid boundary node. A solid node connected at least with one fluid node.
- Interior solid node. A solid node not connected to any fluid node.

A link between a fluid boundary node and a solid boundary node is called a boundary link. The surface of a solid particle is assumed to be located in the middle of the boundary links. Clearly, the stepwise lattice representation of the surface of a spherical particle is neither accurate nor smooth unless a sufficiently small lattice spacing is used. More seriously, when the particle is in motion, its boundary

nodes will continually change, so an effective algorithm needs to be in place to update the boundary nodes at each time step.

For modelling the interaction between a moving particle and fluid Ladd [60] proposed a modification to the original bounce-back rule so that the movement of a solid particle can be accommodated. For a given boundary link i, the modified "no-slip" rule is given by

$$f_{-i}(\mathbf{x}, t+1) = f_i(\mathbf{x}, t) + \alpha_i \mathbf{x}_i \mathbf{v}_b \tag{2.13}$$

where α_i is a parameter calculated by several hydrodynamic quantitities and $\mathbf{v}_b$ is the velocity in the middle of the boundary link i computed as combination of the translational and angular velocities at the mass centre of the solid particle. This model is a very general technique for simulating solid–fluid in which its most important feature is that the computational cost scales linearly with the number of particles. This method combines Newtonian dynamics of the solid particles with a discretized Boltzmann equation for the fluid phase. The many-body hydrodynamic interactions are fully accounted for, both in the creeping-flow regime and at higher Reynolds numbers. Brownian motion of the solid particles arises spontaneously from stochastic fluctuations in the fluid stress tensor, rather than from random forces or displacements applied directly to the particles.
From the collision rule, the impact force on each solid particle from the link can be computed and from them the total hydrodynamic force exerted on the particle is obtained by summing up the forces of all the related boundary links.

Another approach available for modelling the interaction between a moving particle and fluid is the immersed moving boundary (IMB) method, which is a general numerical technique for the modelling of interaction between fluid and deformable structures. The LB algorithm is modified to include a term that depends on the percentage of the cell saturated with fluid. The method is useful for modelling suspended obstacles that do not conform to the grid. Another application is to simulations of flow through reconstructed media that are not easily segmented into solid and liquid regions. The basic ideas behind this approach of Noble and

Torczynski [61] include the establishment of a more accurate and smooth lattice representation of solid particles to reduce the fluctuation of the computed hydrodynamic forces, as well as the modification of the fluid density distribution at the nodes covered by a solid particle to enforce the "no-slip" condition. It introduces a control volume/cell for each lattice node and a local fluid/solid ratio is also defined, which is the area fraction of the nodal cell covered by a particle.
Then, the LB equation for those lattice nodes (fully or partially) covered by a solid particle is given by

$$f_i(\mathbf{r}+\mathbf{c_i},t+1)-f_i(\mathbf{r}+\mathbf{c_i},t)=-\frac{1}{\tau}(1-\beta)\left(f_i(\mathbf{r},t)-f_i^{eq}(\mathbf{r},t)\right)+\beta {f_i}^m \quad (2.14)$$

where β is a weighting function depending on the local fluid/solid ratio and ${f_i}^m$ is an additional term that accounts for the bounce back of the non-equilibrium part of the distribution function. In this way, the total hydrodynamic force exerted on a particle over n particle-covered nodes can be computed.

2.5 Squirmer Model

This model considers a spherical particle, with radius equal to R, with a fixed director that moves with the particle, $\widehat{\mathrm{e}}$. The internal activity of the particle generates an axysimmetric velocity at its surface, which produce the self-driven movement of the particle. This velocity can be written in terms of two independent terms, one radial v_r and another polar v_θ. Both components can be written as the special functions [52-56]:

$$u_r|_{r_s=R}=\sum_{n=0}^{\infty}A_n(t)P_n\left(\frac{\widehat{\mathbf{e}}\cdot\mathbf{r}_s}{R}\right) \quad (2.15)$$

$$u_\theta|_{r_s=R}=\sum_{n=0}^{\infty}B_n(t)V_n\left(\frac{\widehat{\mathbf{e}}\cdot\mathbf{r}_s}{R}\right) \quad (2.16)$$

where $\mathbf{r}_s$ represents the position vector with respect to the squirmer's center of mass, which is always pointing to the particle surface and thus $r_s=|\mathbf{r}_s|=R$. $\widehat{\mathrm{e}}$ describes the intrinsic self-driven direction ($|\widehat{\mathrm{e}}|=1$), which moves rigidly with the particle and determines the direction along which a single squirmer will displace. P_n stands for the n-th order Legendre polynomial and V_n is defined as [65]

$$V_n(\cos\theta) = \frac{2}{n(n+1)} \sin\theta P_n'(\cos\theta) \tag{2.17}$$

Note that $\cos\theta = \frac{\widehat{\mathbf{e}}\cdot\mathbf{r_s}}{R}$ if θ is the angle between the vectors $\widehat{\mathbf{e}}$ and $\mathbf{r_s}$.

$A_n(t)$ and $B_n(t)$ are the amplitudes of the radial and polar components of the axisymmetric velocity imposed at the particle surface. We will disregard the radial changes of the squirming motion, $A_n(t) = 0$, in this way the velocity field generated by a squirmer will depend only on the polar part of the slip velocity and not in the size of the squirmer. We are going to calculate the approximation of the series up to the third order but considering that the frequency of the impulse is much greater than the proper time of the movement, so that the temporal dependence of the amplitude $B_n(t)$ can be replaced by the constant value of the average B_n.

n	$P_n(\cos\theta)$	$V_n(\cos\theta)$
0	1	0
1	$\cos\theta$	$\sin\theta$
2	$\frac{1}{2}(3\cos^2\theta - 1)$	$\cos\theta\sin\theta$

$$u_\theta|_{r_s=R} = B_1 \sin\theta + B_2 \cos\theta \sin\theta \tag{2.18}$$

Another feature in this squirmer model is that squirmer swims in a non-inertial medium, hence the velocity $\mathbf{u}$ and pressure p of the fluid are given by the Stokes and continuity equations:

$$\begin{aligned} \nabla p &= \nu \nabla^2 \mathbf{u} \\ \nabla \mathbf{u} &= 0 \end{aligned} \tag{2.19}$$

Taking in count the boundary conditions specified by the slip velocity in the surface of its body and the constraints we specified above, we have that the mean fluid flow induced by squirmer, from the general solution for $n < 3$, is the vector field over a point with position $\mathbf{x}$ and in a time t given by the equation

$$U(\mathbf{x},t) = -\frac{1}{3}B_1\left(\frac{R}{r}\right)^3\widehat{\mathbf{e}} + B_1\left(\frac{R}{r}\right)^3(\widehat{\mathbf{e}}\cdot\widehat{\mathbf{r}})\widehat{\mathbf{r}} \qquad (2.20)$$
$$-\frac{1}{2}B_2\left(\frac{R}{r}\right)^2(3(\widehat{\mathbf{e}}\cdot\widehat{\mathbf{r}})^2-1)\widehat{\mathbf{r}} + o\left(\left(\frac{R}{r}\right)^4\right)$$

where $\mathbf{X_p}$ is the position of the center of mass of the particle, $\mathbf{r} = \mathbf{x}(\mathbf{t}) - \mathbf{X_p}(\mathbf{t})$, $r = |\mathbf{r}|$ and $\widehat{\mathbf{r}} = \frac{\mathbf{r}}{r}$. The coefficient $B_1 > 0$ determines the self-propulsion velocity, $V_p = \frac{2}{3}B_1$, and B_2 is related to the amplitude of the stress exerted by the microswimmer on the surrounding fluid. The sign of B_2, or equivalently of the ratio $\beta = \frac{B_2}{B_1}$, determines the classification [65-66]:

- Pushers ($\beta < 0$) obtain their thrust from the rear part of their body.
- Pullers ($\beta > 0$) obtain their thrust from the front part of their body.

2.6 Ludwig Code

Lattice Bolzmann Method (LBM) is the most popular theory to use in computer simulations because it is solved locally and i t has high degree of parallelization, hence it is ideal for parallel machines (computational clusters). In this thesis we have performed several simulations using the Ludwig Code, which is a LB open-source code for $D3Q19$ lattice [58] and some results are presented in chapters 3 and 4 of this work.

Ludwig is a code written in ANSI C based on the LBM for simulating complex three-dimensional fluids through a set of routines and communications [41]. Time evolution of modelled quantities takes place on a fixed regular discrete lattice. The preferred method of dealing with the corresponding equations is by using finite difference. However, for the case of a binary fluid, a two-distribution lattice Boltzmann approach is also maintained for historical reference. With this code it is possible to configure multiple models with different values of free energy and other parameters. This is a particularly interesting code because given the relative simplicity of execution in relation to the power of simulation is ideal to be able to draw

physical conclusions without having to deal with a complicated programming situation, so that the user may concentrate on the physics of the problem, rather than on parallel computing issues. *Ludwig* is structured as a library of preconfigured models that can be affected at the parametric level through the input file [57]. The underlying physics is within the framework of active nematics and the program allows creating periodic boundary conditions, interaction between colloids in suspension, liquid crystals (using the Landau-de Gennes equations [21]) and binary fluids.

Ludwig has been developed with a modular and hierarchical structure in mind. The current version of the package is composed of 258 functions (over 25,000 lines of code) split in three main components: models (D3Q19, D3Q15), common and utilities. The code has been developed over a number of years to address specific problems in complex fluids. The underlying hydrodynamic model is based on the lattice Boltzmann equation [41]. This itself may be used to study simple (Newtonian) fluids in a number of different scenarios, including porous media and particle suspensions. However, the code is more generally suited to complex fluids, where a number of options are available, among others: symmetric binary fluids and Brazovskii smectics, polar gels, liquid crystals, or charged fluid via a Poisson-Boltzmann equation approach. These features are added in the framework of a free energy approach, where specific compositional or orientational parameters are evolved according to the appropriate coarse-grained dynamics, but also interact with the fluid in a fully coupled fashion.

Users control the operation of the code via a plain text input file; output for various data are available. These data may be visualised using appropriate third-party software. Specific diagnostic output may require alterations to the code. Potential users should note that the complex fluid simulations enabled by Ludwig can be time consuming, prone to instability, and provide results which are difficult to interpret. By default, the run time expects to find user input in a file located in the current working directory. When an input file is located, its content is read by a single MPI task, and its contents then broadcast to all MPI relevant tasks. Input file consists of a series of key values, each of which controls at least one parameter in the code,

such as system size, number of cycles in iteration, output file frequency, parallel decomposition data, etc. These key values can be scalar, vector, tensor, or floating point nomenclature numbers. If some key values do not need to be present for a particular program run, the code uses default values that affect execution as little as possible. Input file also includes explanations and clarifications throughout its script. This file must be in the same directory as the *Ludwig.exe* executable, which was previously compiled using serial or parallel configuration. The execution of the executable produces a set of data files also in the same directory, if the decomposition has been used in parallel of the calculations, that is to say, if they have been done by different volumes of the grid, it will be necessary a post-production data procedure to recombine the results of the different volumes. As a convenience, it is possible to specify that sets of plane walls are present in the system in one or more co-ordinate directions with periodic conditions. The code produces a series of output files that give information about the velocity field, density, momentum, or integrated free energy. Precisely, free energy is possibly the most categorical parameter of a given model [41][58].

We have performed simulations using a D3Q19 lattice, which includes moving particles via domain decomposition and message passing using the message passing interface MPI. A simulation in a cubic box with an edge length of $512 \times 512 \times 512$ (largest ones that we have done) needs a RAM memory of almost 20 Gb and it the requirement of memory grows linearly with the growth of the volume.
Due to the magnitude of the system size required, it became obvious from the early stage of the design that Ludwig would have to be parallelized in order to provide the required scalability. Fortunately, the symmetry of the underlying cubic lattice guarantees a uniform data distribution and hence an equal amount of computations per lattice site. Indeed, the collision and propagation stages will take place over all lattice sites, which restricts possible causes of load imbalance to the introduction of solids objects non-uniformly distributed across the simulation box. This pseudo-uniform distribution of the computations added to the intrinsic locality of the LB algorithm made Regular Domain Decomposition the most suitable decomposition strategy. In this approach, the data is geometrically decomposed in equal volumes, which are then distributed to each processing element.

Although periodic boundary conditions are applied to the model by default, these can be modified by explicitly adding solid surfaces at the boundaries. In the previous subsection we have shown how to add them, ensuring stick boundary conditions. This is enough for a mono-component simple fluid. However, for complex fluids it is also in general necessary to specify the behaviour of additional fields at solid boundaries, whether these are at the edges of the system or internal boundaries between fluid and solid phases. The implementation of static solid objects and moving walls in parallel is also quite simple making it suitable to exploit the capabilities of supercomputers, with a modular structure, which allows its use without the need to know its computational details.

CHAPTER

3

Diffusion and polar order in active particles suspensions

In this chapter an exploration of the (ϕ, β) parameter space has been performed for evidence of collective behaviour in several simulations with microswimmers using Ludwig code on a cubic grid of size $128 \times 128 \times 128$, $256 \times 256 \times 256$ and $512 \times 512 \times 512$.
ϕ represents the concentration of particles in the fluid and β is the relationship between the order parameter and the self-propulsion velocity for each particle. Some graphical results are shown and, through their interpretation, our objective is to find numerical evidence of how these parameters affect the behaviour of the fluid, specifically to mean squared displacement of particles and to spontaneous increase in the level of collective orientation.

3.1 Introduction

This study was performed from the results of several simulations with Ludwig code with a size of 400000 iterations at least, carried out in the Albeniz cluster of the Fundamental Physics department of the Barcelona University. We want to explore

the parameter space (ϕ, β). ϕ is the bacteria (microswimmers for us) volume fraction, for N spheric particles with radius 2.5 into a cubic grid of length equal to 128 units. $\beta = \frac{b_2}{b_1}$ is the ratio between b_1, which corresponds to a parameter of the self-propelled (proper) particles velocity , and b_2, which corresponds to a parameter of particles orientation (in a nematic sense)

Differences are expected to be observed between pushers ($\beta < 0$) and pullers ($\beta > 0$), due to the differentiated behaviour at a dynamic level that has been observed in other studies [43]. In this sense, the most significant difference that we have detected, emerges in the dependence of the particle's mean squared displacement (MSD) on the swimmers concentration: in the pullers case a sharp increase is observed for lowers values of ϕ as a result of a clear exponential change of the underlying behaviour. This surprising effect is associated with an increase in the degree of orientation (polar order) of the system that is much higher than the rest of the simulations, even though their b_2 values are the same.

The reference [44] ascribe this change in MSD behaviour to the formation of large scale coherent motions, so the formation of clusters is also expected. This situation could produce collective movements of sets of the particles grouped in significant percentage fractions and should be possible to detected them on the parameter space (ϕ, β).

Finally, some results of our simulations reproduce behaviours published in a previously article [44], helping to verify and expand the knowledge about some essential aspects of the phenomenon.

3.2 Mean Square Displacement

Mean squared displacement (MSD),

$$\langle \Delta r^2 \rangle(t) = \frac{1}{N} \sum_{i=1}^{N} |\mathbf{r}_i(t) - \mathbf{r}_i(0)|^2$$

is calculated in order to quantify the movement capacity of the particles within the grid and to be able to study how it is affected by concentration ϕ and level orientation b_2. Some differences in the behaviour of pullers ($\beta > 0$) and pushers ($\beta < 0$) are also studied.

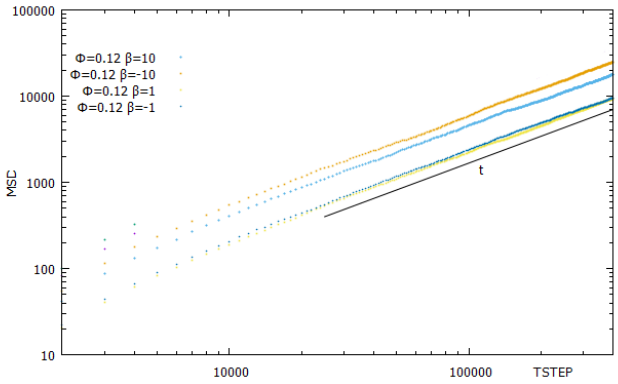

Figure 3.1: *MSD calculated for different β values ($b_1 = 0.01$ $b_2 = \pm 0.01, \pm 0.1$) with $\phi = 0.12$ and 4×10^5 iterations. MSD increase in relation to the parameter b_2. No clear differences between pullers and pushers are observed.*

In statistical mechanics, the mean squared displacement is a measure of the deviation of the position of a particle with respect to a reference position over time.

3.2.1 Variation of β parameter

We performed several simulations at cluster Albeniz to study how the variation of β affects the MSD. All of them were done it in a cubic grid with size 128^3 and $\phi = 0.12$.

In FIG. 3.1 there are β values that have been obtained by varying b_2 for a constant value b_1. Increasing the orientation level also results in an increase in MSD. From the four curves with $b_1 = 0.01$ ($\beta = \pm 1, \pm 10$) it is easy to observe that MSD increase slowly in relation to the parameter b_2.

Another characteristic of these curves is that they point to the possibility that a higher level of orientation produces a clearer difference between the corresponding pushers and pullers because the larger b_2, the greater the separation between the corresponding pullers and pushers lines seems to be for the same value of $|\beta|$.

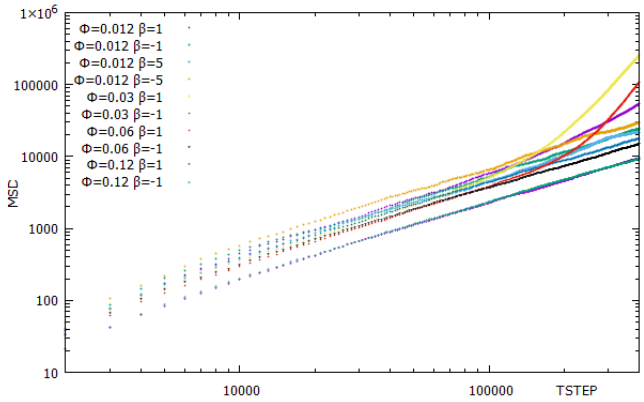

Figure 3.2: *MSD calculated for different ϕ values and for pullers and pushers $\beta = \pm 1$ ($b_2 = \pm 0.01$). A transition from a diffusive regime ($\langle \Delta r^2 \rangle \sim t$) to a ballistic regime ($\langle \Delta r^2 \rangle \sim t^2$) can be obseved only for pullers. This effect is stronger for $\phi = 0.03, 0.06$*

3.2.2 Variation of concentration

The most surprising result of how many are shared in this chapter is found in the calculation of MSD for different concentrations, ϕ, keeping constant $|\beta| = 1$ ($b_1 = 0.01$, $b_2 = \pm 0.01$). It can be seen that for low concentrations in the pullers case there is a clear change in the increasing trend of the curve showing a strong asymmetry between pullers and pushers (FIG.3.2).

In FIG.3.2 a clear effect of increasing the mean displacement of puller particles is shown at low concentration and with relatively low orientation levels. It is observed, for a concentration $\phi = 0.012$, that the MSD increases with a change in slope if $\beta = 1$, but if $\beta = -1$ this phenomenon is not present. This change from a diffusive regime ($\langle \Delta r^2 \rangle \sim t$) to a ballistic regime ($\langle \Delta r^2 \rangle \sim t^2$) is stronger in the case of $\phi = 0.03$ or $\phi = 0.06$. Likewise, for the lowest concentration, by increasing $\beta = \pm 5$ through the orientation parameter, $b_2 = \pm 0.05$, any change in the increasing trend of MSD disappears.

In the following panel (FIG:3.3) it is possible to observe each isolated case of interest and appreciate more precisely the position of the crossover. The immediate

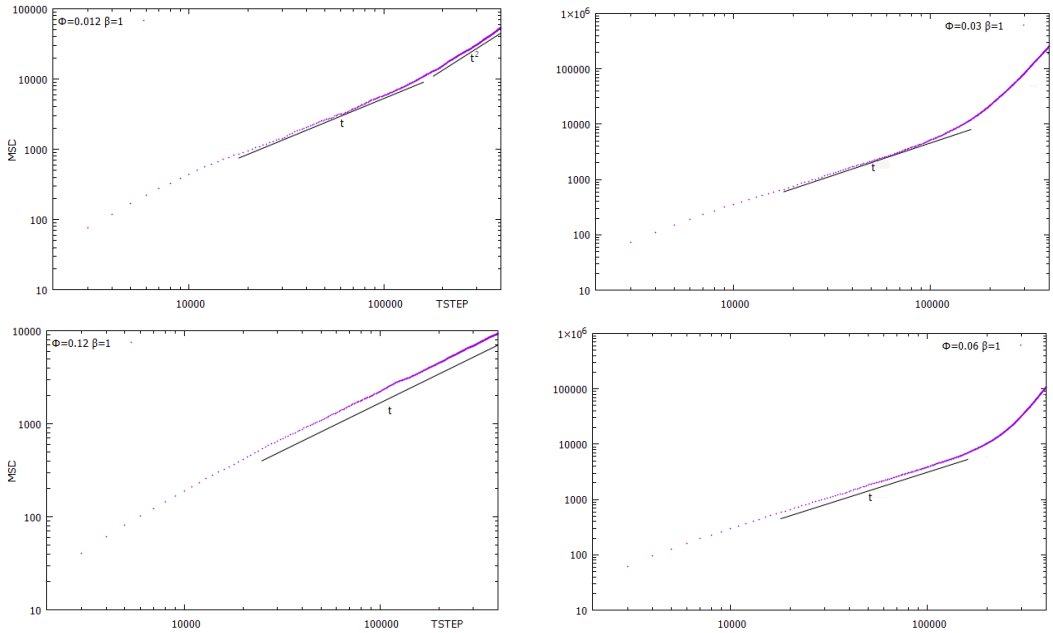

Figure 3.3: *MSD as a function of concentration, ϕ. It is possible to observe each isolated case of interest and appreciate more precisely the position of the crossover.*

questions to be solved is to know how the size of the grid affects this phenomenon and, if it is prolonged in time, another regime traversal will take place. However, first of all, it is interesting to see if this abrupt change in the displacement of the particles is due to or has caused any change in the mesoscopic properties of the particles.

3.3 Polar order

To better understand the corssover explained in previous section and assuming that a higher orientation level favours the displacement of the particles, the mean orientation, $P\left(t\right)$, is calculated for different β and ϕ values according to the expression:

$$P\left(t\right) = \frac{\left\| \sum_{i=1}^{N} \mathbf{e}_i\left(t\right) \right\|}{N} \tag{3.1}$$

where $\mathbf{e}_i(t)$ represents a 3-dimensional orientation vector of a particle i at the time step t of execution of a simulation with N particles for a determined printed

iteration step, t.

At long-times, the suspension reaches a steady state $P(t >> 0) = P_\infty$. If $P_\infty = 1$ the system is completely polarized (all squirmers point in the same direction), while $P_\infty \sim 1/\sqrt{N}$ means the system is isotropically oriented [77].

In figure 3.4 it can be seen that simulations that behave differently from the rest in regard to MSD also behave differently for $P(t)$. In FIG. 3.5 we can see that the simulations that presented a crossover when studying the evolution of their MSD, now they also have a much longer transitory state, reaching a value of the mean square orientation much higher than the rest(FIG. 3.4). In these cases, the P_∞ parameter is calculated for the times within the steady state. These values of ϕ and β show a transition to the ballistic regime at the same point that the steady state of the mean orientation, $P(t)$, is reached.

The fact is that a degree of ordering has been generated spontaneously (not through the execution parameters of the program) which greatly facilitates the displacement of the particles as they are dragged by the fluid. This effect only occurs in the case of pullers.

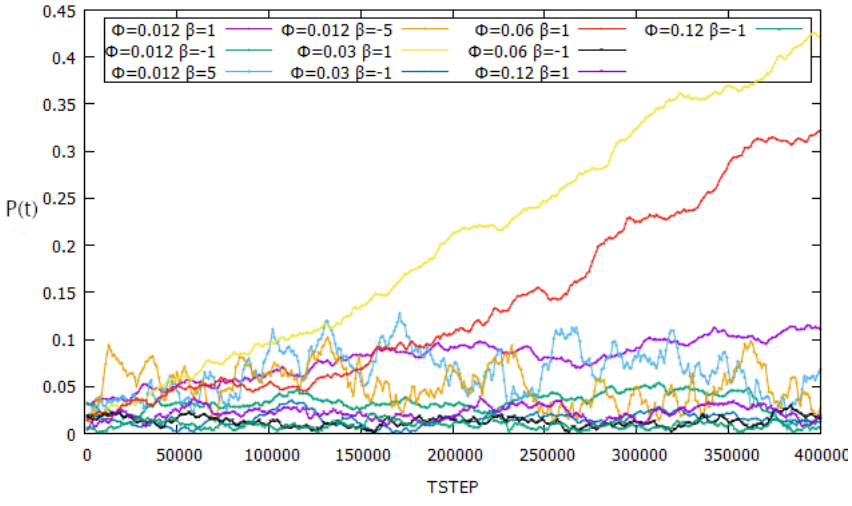

Figure 3.4: *$P(t)$, calculated for diferent ϕ and β. TIME STEP represents each simulation step as a time variable.Simulations that behave differently from the rest in regard to MSD also behave differently for $P(t)$. The increase of the orientation parameter b_2 (β) does not seem to have any effect in relation to the polar order.*

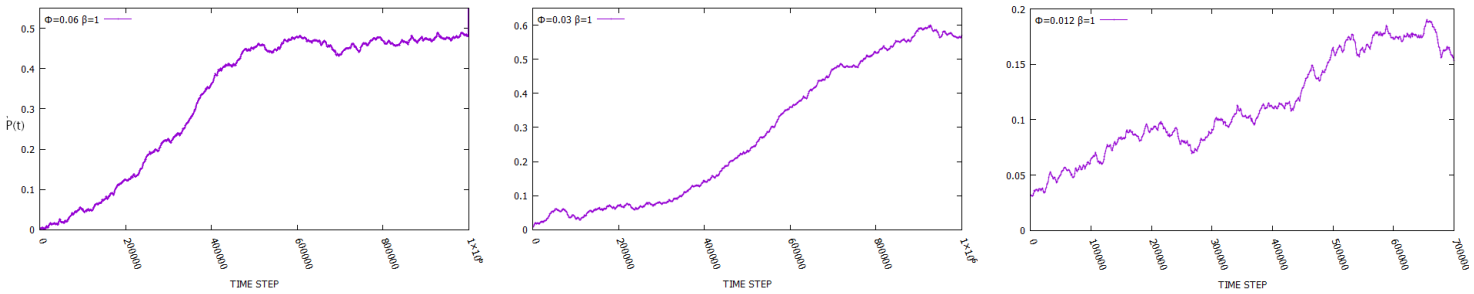

Figure 3.5: *Different values of the polar order, P_∞, (calculated for the times within the steady state) depending on the concentration. From left to right $P_\infty \sim 0.5, 0.6, 0.2.P_\infty$. These values of ϕ and β show a transition to the ballistic regime at the same point that the steady state of the mean orientation, $P(t)$, is reached. Other simulations with other values of ϕ and β show no increase in $P(t)$.*

Polar order parameter P_∞ is calculated for $\phi = 0.12$ and different values of β in figure 3.6 The plot does show some similarity with the reference [45][66] in presence and position of the peak.

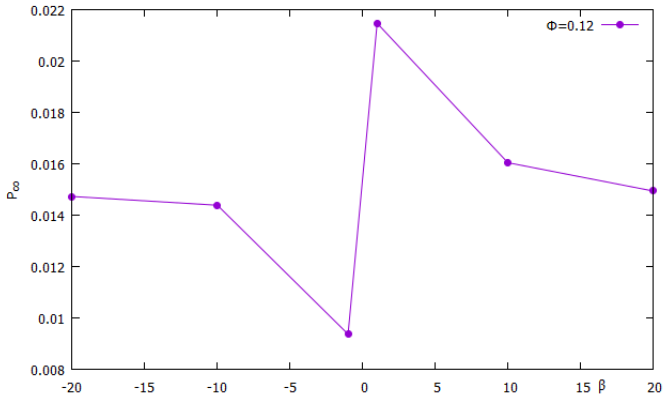

Figure 3.6: *Polar order parameter, P_∞, for different β values and $\phi = 0.12$ Note the peak for β values around one.*

in FIG. 3.7 it can be seen that, for other concentration values, P_∞ reach values similar to that of the reference [45] for $\beta = 1$.

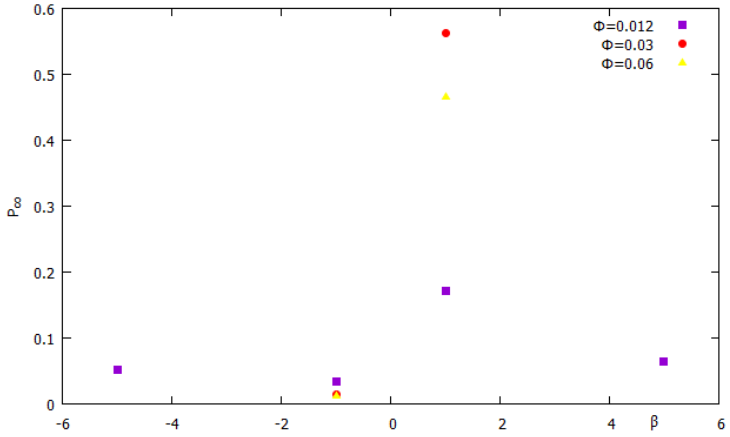

Figure 3.7: *Polar order parameter, P_∞, for different ϕ values. Note the peak for β values around one.*

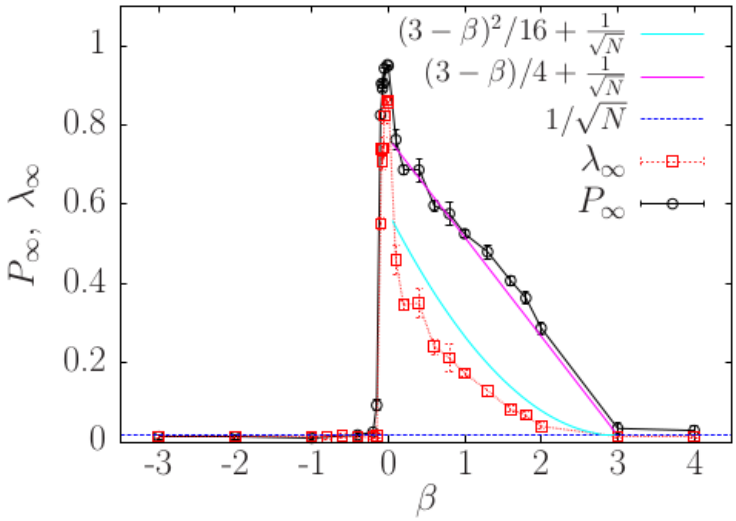

Figure 3.8: *Long-time polar P_∞ and nematic order λ_∞ parameter for different values of β ranging from -3 to 4. P_∞ is plotted with black circles, while λ_∞ is represented by red squares. Particles with isotropic orientation will have a $P_\infty \sim 1/\sqrt{N}$ hence we also show the blue dashed line that represent $1/\sqrt{N}$. P_∞ has a linear behaviour in the region where $0 \leq \beta \leq 3$, similarly λ_∞ has a quadratic behaviour in the same region of β, thus we plot also this linear and quadratic behaviour with a pink and cyan curve respectively.*

In Fig. 3.8 (*provided by Dr. Francisco Alarcón*) we show the value of P_∞ (black circles) as a function of β. We observe that pushers with $\beta \lesssim -1/10$ are isotropically oriented ($P_\infty \sim 1/\sqrt{N}$). For $\beta > -1/10$, P_∞ increases abruptly, signalling

the emergence of a polar order, up to a maximum $P_\infty \approx 1$ at $\beta = 0$, and then decreases again, linearly. For $\beta \geq 3$ the suspension is isotropic again.

3.4 Clustering

Squirmers can develop another interesting collective phenomenon, which is the emergence of flocking: clusters of particles moving coherently together can spontaneously aggregate, disgregate and aggregate again in time. These processes generate particle density fluctuations across the system [45]. In this situation, according to the bibliography reference [44], it would be reasonable to think about the formation of clusters or flocks, but the data do not show the existence of either of the two things. particles are distributed forming a cluster around 60% and the rest is distributed in a residual way in more than ten different groups.
The formation of this macroscopic cluster is driven by the competition between the hydrodynamic interactions (hence, the swimming characteristics), responsible of particle reorientations, and the volume fraction, controlling the particle collision rates.

3.5 Root Mean Square fluid velocity

A result that does agree with the bibliography is the study of average root-mean-square fluid velocity, U_{RMS}, analysed following the procedure described in reference [44] with the aim to compare the results with the reference's image where U_{RMS} is represented, as a function of the swimmer concentration. There is an increasing trend as might be expected (FIG. 3.9) but with a much lower energy level and without observing the characteristic slope change that is showed in the reference because it may not have high enough particle densities.

3.6 Super-Ballistic Diffusion

The transition to the long time ballistic regime, driven by the macroscopic flock formation, can lead to transient super-ballistic diffusion. To highlight this behaviour,

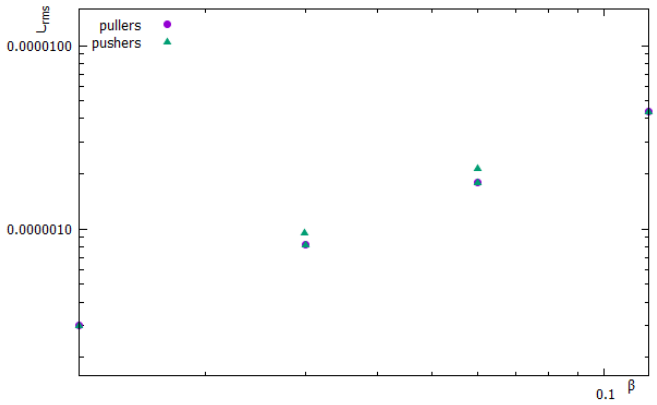

Figure 3.9: *U_{rms} of the fluid for different ϕ values for pullers and pushers*

we report in Fig. 3.10 the local slope of the MSD, defined as

$$\gamma(t) = \frac{d\log\langle\Delta r^2\rangle}{d\log t}$$

together with the time evolution of the polar order parameter $P(t)$, for pushers ($\beta = 1$) at $\phi = 0.06$ in a smaller system ($L = 128$).

As long as $P(t) \ll 1$ (no polar order), the particle dispersion is diffusive ($\gamma \sim 1$). The growth of $P(t)$ is followed by a steep increase of the local slope, which even overshoots the ballistic value ($\gamma = 2$), reaching $\gamma \sim 4$, as $P(t)$ approaches the steady state value P_∞, and then relaxes asymptotically to the ballistic regime again.

3.7 System size analysis

Next, we will analyse how the size of the grid affects the results. For this, a simulation has been carried out in the machine Mare Nostrum of Spanish Supercomputer Net (RES) with a grid of size $512 \times 512 \times 512$, a concentration of $\phi = 0.012, 0.06, 0.12$ and $\beta = 1, -5$ ($b_1 = 0.01, b_2 = 0.01, -0.05$).
As can be seen in the figures, the increase in the size of the grid seem to change

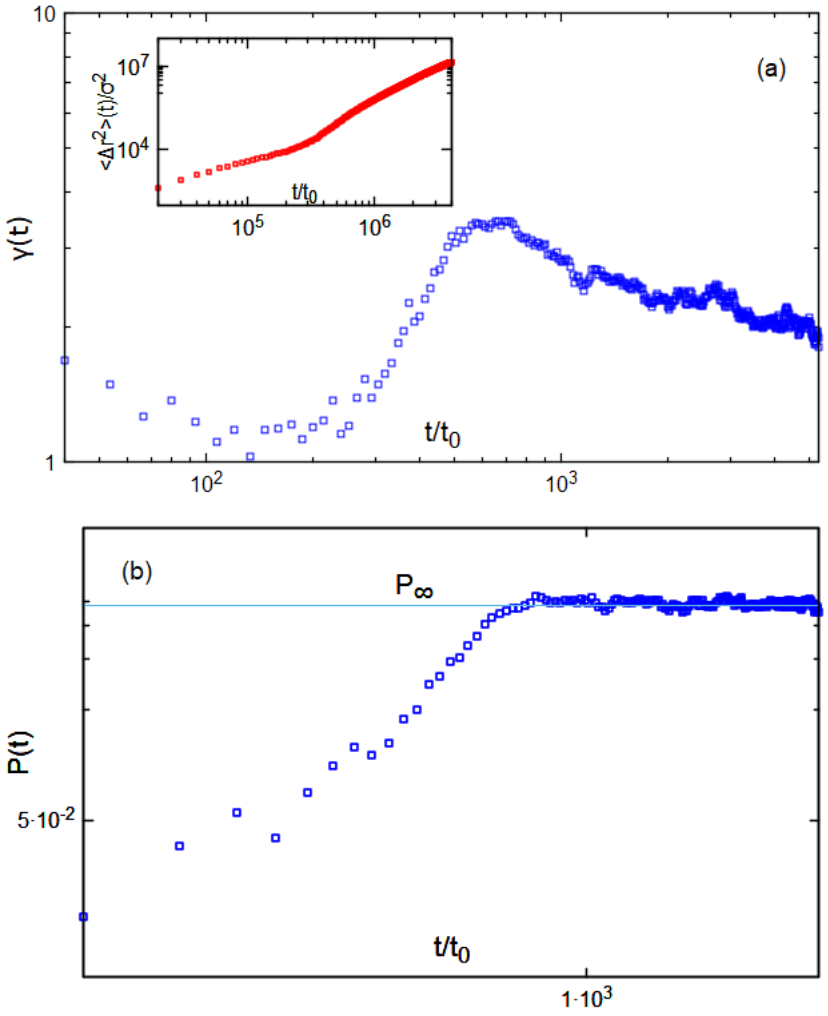

Figure 3.10: (a) Local slope, $\gamma(t) = \frac{d\log\langle\Delta r^2\rangle}{d\log t}$, for squirmers with $\phi = 0.06$ and $\beta = 1$ in a system of size 128^3. Inset: MSD shows a second cross-over at long times. (b) Polar order parameter, $P\left(t\right) = \frac{1}{N}\left|\sum_{i=1}^{N}\mathbf{e}_i(t)\right|$.

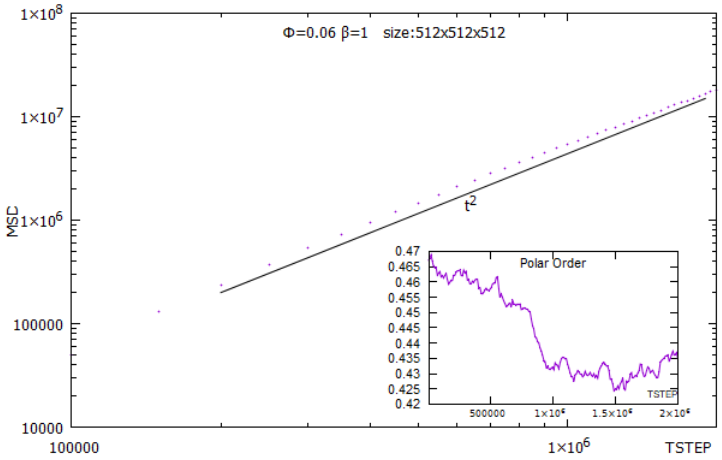

Figure 3.11: *MSD calculated for $\phi = 0.06$ with $\beta = 1$ ($b_2 = 0.01$) in a grid of size $512 \times 512 \times 512$ and 2×10^6 iterations achieving a ballistic regime. INSET: $P(t)$ does not reach a steady state in which polar order can be measured, a continued decrease is observed.*

some substantial aspect in the behaviour of the particles in terms of displacement dynamics. The figures corresponding to a concentration $\phi = 0.06$ and $\beta = 1$ $(b_1 = 0.01, b_2 = 0.01)$ for grid sizes $512 \times 512 \times 512$ and $256 \times 256 \times 256$ (FIG. 3.11, FIG. 3.15) show a local slope equal to 2. Even despite a quantitative difference in respect to the case $128 \times 128 \times 128$ for the same concentration and values b_1 and b_2 (FIG. 3.3), qualitatively it should be noted that there is still a clear deviation from the linear growth of MSD for this concentration in all grid sizes. Furthermore, comparing the same figures with the values in figure 3.5 , it can be seen that the polar order increases to values close to 0.5 in the three sizes of the grid.

The rest of the figures correspond to concentrations $\phi = 0.12, 0.06, 0.12$ with $\beta = -5$ $(b_1 = 0.01, b_2 = -0.05)$ show the local slope close to one (FIG. 3.12, FIG. 3.13, FIG. 3.14) like most of the curves presented earlier in the figures at a grid size of $128 \times 128 \times 128$ (FIG. 3.1, FIG. 3.2)

Therefore, according to these results it can be said that in the case $\phi = 0.06$ and $\beta = 1$ $(b_1 = 0.01, b_2 = 0.01)$ there is a change in the behaviour of the particles that are reflected in a significant increase and an essential change in behaviour in the time evolution of the mean square displacement accompanied by an increase in the polar order of the system up to a value close to 0.5.

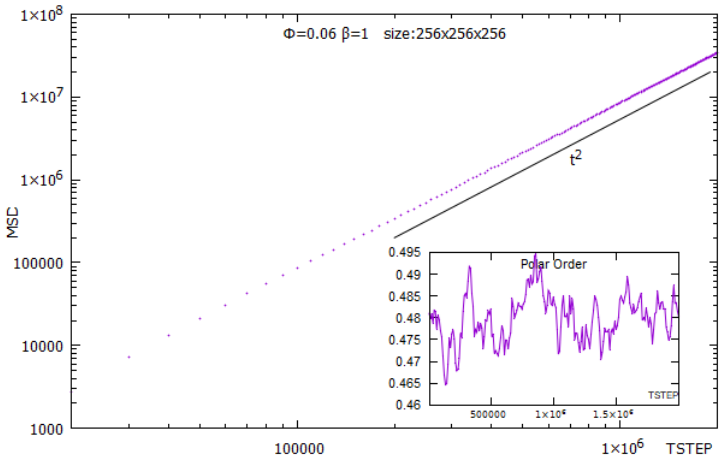

Figure 3.12: *MSD calculated for* $\phi = 0.06$ *with* $\beta = 1$ *(*$b_2 = 0.01$*) in a grid of size* $256 \times 256 \times 256$ *and* 2×10^6 *iterations achieving a ballistic regime. INSET:* $P(t)$ *reach a steady state in which polar order can be measured about 0.5*

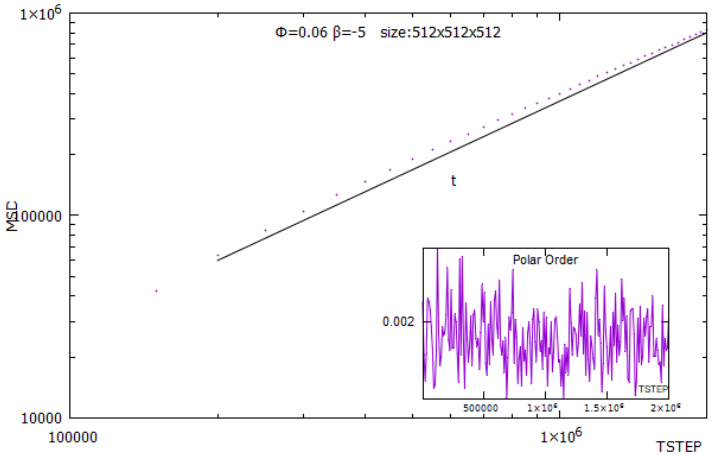

Figure 3.13: *MSD calculated for* $\phi = 0.06$ *with* $\beta = -5$ *(*$b_2 = -0.05$*) in a grid of size* $512 \times 512 \times 512$ *and* 2×10^6 *iterations. It stay in a diffusive regime. INSET: P(t) remains at values close to zero.*

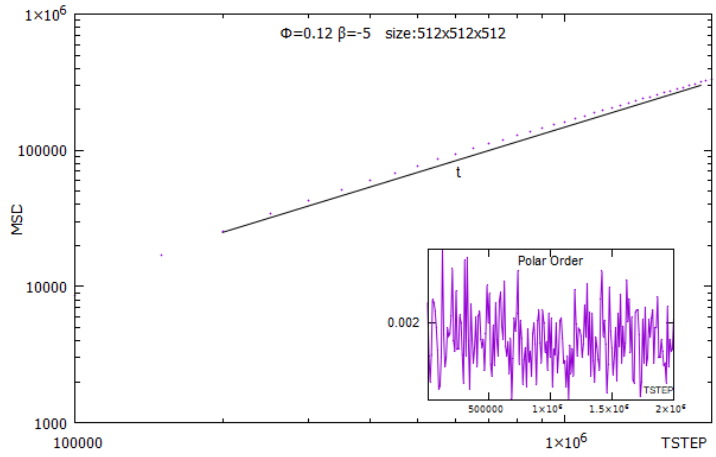

Figure 3.14: *MSD calculated for* $\phi = 0.12$ *with* $\beta = -5$ *(*$b_2 = -0.05$*) in a grid of size* $512 \times 512 \times 512$ *and* 2×10^6 *iterations. It stay in a diffusive regime. INSET: P(t) remains at values close to zero.*

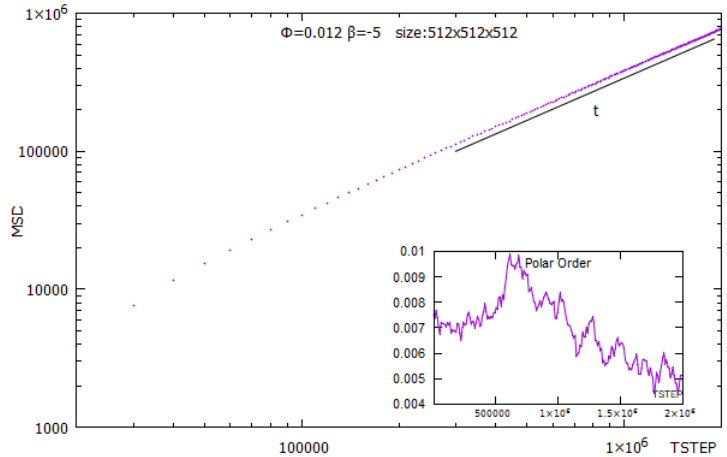

Figure 3.15: *MSD calculated for* $\phi = 0.012$ *with* $\beta = -5$ *(*$b_2 = -0.05$*) in a grid of size* $256 \times 256 \times 256$ *and* 2×10^6 *iterations. It stay in a diffusive regime. INSET: P(t) remains at values close to zero.*

3.8 Conclusions of the chapter

We have used Lattice-Boltzmann methodology to carry out simulations of semi-dilute squirmer suspensions, where hydrodynamic interactions are taking in count explicitly. A substantial change in mean squared displacement, MSD, is observed for certain relatively low concentrations of swimmers in the puller case. This increase is also related to a spontaneous increase in the level of particles orientation. Our explanation is that higher concentrations favour particles collisions and increase the number of short displacements, then all these truncated movements, that do not manifest in kinetic form, must contribute to the internal energy of the system. So the observed behaviour of strong increase in MSD is due to the fact that a greater part of the internal energy of the system is transformed into kinetic energy by an increase in the orientation level.

In the next section of this work, the energy spectra of the simulations are explored with the aim of finding quantitative evidence of this supposed accumulation of internal energy as a result of an increase in the dynamic stress.

There is a point in the parameter space (ϕ, β) that favours an almost resonant increase in MSD related to spontaneous orientation of the suspended particles as a way to relax the tension of the fluid transforming the internal energy accumulated into kinetic energy.

In general, we observe that aligned suspensions develop a multi-crossover Mean Square Displacement, where suspensions reach a super-diffusive motion at long-times. Our group has presented a publication on this subject in which results are offered in a more extensive way [64]. Ishikawa and Pedley [62][63] also found anomalous diffusion for small $|\beta|$, they studied the spreading of squirmers in non-uniform suspensions and they said that this ordering phenomenon may be interpreted as a taxis towards lower cell concentration.

CHAPTER

4

Active Turbulence

In this chapter, the energy spectrums, $E(k)$ of several large scale direct numerical simulations are analyzed

$$E(k) = \frac{1}{2}\overline{\left\langle \widetilde{\mathbf{u}^*} \cdot \widetilde{\mathbf{u}} \right\rangle} \tag{4.1}$$

where $\widetilde{\mathbf{u}}$ is the Fourier transform of the fluid velocity field and the overlined brackets, $\overline{\langle \cdot \rangle}$, indicate a surface integral on spheres of radius k, in spectral space, and time averaging over the statistically stationary state.

Our main purpose is to find indications of energy flows through the different scales (represented by different values of k in the $Forurier$ space), in particular, the flow from the smallest scales (high values of k) towards the largest scales, known as the inverse cascade phenomenon. As a signature of turbulence we expect to observe that, as the volume fraction decreases , the energy spectrum at low wavenumber should be broadened, distributing the energy of the system in an increasingly homogeneous way through an increasing range of scales until reaching the diffusive level where a sudden fall would occur. In particular, in the limit of $\phi \to 0$ one should observe $E(k) \sim$ const., with a steep decay at high k [44].

This chapter presents the results obtained in different simulations from the variation of the orientation parameter and the concentration of the solution. However, first there is a brief introduction to the theoretical framework and a reminder of the basic principles governing isotropic hydrodynamic turbulence.

4.1 Introduction

In active matter, the characteristic activity of some kind of systems called wet, may be expressed not in autonomous motion but in forces applied by agents on the medium they are immersed in. This kind of systems are complex and deterministically unstable.
On a basic level of description, both the medium and the agents can be lumped into a continuous active fluid, where the agents are characterized only by their symmetry and the matching action. A particle with nematic symmetry can exert a force along its axis that produce a motion which we can consider slow, so inertia is neglected. Then the model is based on the Stokes equation of viscous motion supplemented by the effects of nematic elasticity and activity. The mechanical stress driving passive flows is of external origin; internally, it includes only viscous dissipation. The motion induced by activity is counterbalanced by the elastic stress and dissipated by the bulk and wall friction.
In active suspensions, whatever the origin of activity (which may come from active particles, bacterial suspensions, filaments driven by molecular motors, or living cells), can be modeled by viewing them as homogeneous fluids and solving hydrodynamic equations of motion amended by adding the force exerted by microscopic particles uniformly distributed in the fluid where they are advected by the collectively generated flow. We could say that its local movement is cause and consequence of itself. The continuous approach is justified by the assumption that, similar to passive liquid crystals, the flow and alignment patterns develop on a scale far exceeding the size of individual.

At this point it is impossible not to relate the dynamics, topology and complexity of the behaviour with the inertial turbulence at low Reynolds number. Under

proper parameterization, active matter systems can reproduce these behaviours, receiving the name of active turbulence. Simulations, such as those in the preceding chapter, are carried out on a lattice with the purpose of observing some characteristic that reveals the existence of a turbulent behavior. In this sense, it should be remembered that inertial turbulence is described as a competition between an energy flow from the smallest to the largest scales (inverse cascade) and the opposite process in which the energy flows from the interactions of greater characteristic length towards microscopic type (direct cascade). If the scales are defined through a superposition of Fourier modes, the energy spectrum should show, for different values of the parameters, a variation in the shape that could reveal the existence of energy transmissions through the scales in one or the other sense recording the phenomenon of active turbulence.

4.2 Locally isotropic turbulence

Andrei N. Kolmogorov [1] devoted his research interests to the area of turbulence [2], where his publications from 1941 onwards had a significant influence on the field [1][6][8]. Based on the work of Taylor and Richardson [4][5], he postulated three hypotheses to formulate his theory.

4.2.1 Kolmogorov's first hypothesis

The randomness of a perturbation increases with larger Reynolds numbers, it is a process with an isotropic tendency. However, the boundary conditions mean that perturbations of order L_0, close to the characteristic size of the whole system, cannot be considered isotropic.

Since the influence of the average motion of the fluid decreases with scale, by $\lambda << L_0$ can be considered a locally isotropic turbulence, in a region U_λ far from the borders by sufficiently high Reynolds numbers .

[1] Andrei Nikolayevich Kolmogorov, in addition to making contributions to turbulence and classical mechanics, is known for his work in the theory of probability and topology. He structured the axiomatic system of probability theory, using the language of set theory, and founded the theory of algorithmic complexity.

Variations in perturbations under these scale conditions are significantly faster than global changes in fluid parameters so that it can be considered a quasi-steady state.

$$R = ||x' - x|| << L_0 \; |x, x' \epsilon U_\lambda \Longrightarrow \tau = t' - t = \tfrac{r}{\bar{v}} << T = \tfrac{L_0}{\bar{v}}$$

4.2.2 Kolmogorov's second hypothesis

In a locally homogeneous and isotropic region the fluid is determined solely by the forces of inertia and friction.

Let ε_λ be the energy dissipated per unit mass and unit of time through the scales then how to fulfill $\varepsilon_\lambda \sim \frac{\mu_\lambda v_\lambda^2}{\lambda^2}$, dimensionally $[\varepsilon_\lambda] = L^2T^{-3} \Longrightarrow [\mu_\lambda] = L^2T^{-1}$. At a given scale the energy injected into the perturbation must be equal to the energy dissipated: $\varepsilon_{\lambda_0} \sim \frac{(v_{\lambda_0})^3}{\lambda_0}$ From the dimensional analysis, Kolmogorov defined the following relations corresponding to length, velocity and time of this characteristic scale known as Kolmogorov scale, λ_0

$$\left(\frac{\varepsilon_\lambda \lambda^2}{\mu_\lambda}\right)^{\frac{1}{2}} \sim (\varepsilon_\lambda \lambda)^{\frac{1}{3}} \Longrightarrow \lambda_0 = \left(\frac{\mu_{\lambda_0}^3}{\varepsilon_{\lambda_0}}\right)^{\frac{1}{4}}$$

$$\frac{(v_\lambda)^3}{\varepsilon_\lambda} \sim \left(\frac{\mu_\lambda v_\lambda^2}{\varepsilon_\lambda}\right)^{\frac{1}{2}} \Longrightarrow \qquad v_{\lambda_0} = (\varepsilon_{\lambda_0} \mu_{\lambda_0})^{\frac{1}{4}} \qquad \tau_{\lambda_0} = \frac{\lambda}{v_\lambda} = (\frac{\mu_{\lambda_0}}{\varepsilon_{\lambda_0}})^{\frac{1}{2}}$$

4.2.3 Kolmogorov's third hypothesis

Up to the Kolmogorov scale, λ_0, the energy flow has passed without significant losses from the upper scale L_0. In the inertial range $\lambda_0 << \lambda << L_0$ there is no significant influence of viscosity.

The total constant energy dissipated by the Kolmogorov scale perturbations is of the order of $\varepsilon \sim \frac{v_{L_0}^3}{L_0}$ seeds

$$\lambda_0 \sim \left(\frac{\mu_{\lambda_0}^3 L_0}{v_{L_0}^3}\right)^{\frac{1}{4}} = \left(\frac{L_0^4}{Re^3}\right)^{\frac{1}{4}} = L_0 Re^{-\frac{3}{4}}$$

$$v_{\lambda_0} \sim \left(\frac{v_{L_0}^3 \mu_{\lambda_0}}{L_0}\right)^{\frac{1}{4}} = \left(\frac{v_{L_0}^4}{Re}\right)^{\frac{1}{4}} = v_{L_0} Re^{-\frac{1}{4}}$$

Kolmogorov's characteristic length and velocity decrease with increasing Reynolds number,Re, that is, the radius of influence of the frictional force decreases with increasing Re.

Navier-Stokes equations are invariant under scale transformations

$$x_\lambda \Rightarrow x\lambda \qquad v_\lambda \Rightarrow v\lambda^r \qquad t_\lambda \Rightarrow t\lambda^{1-r}$$

Then, if in the inertial range ε is constant at any scale:

$$\varepsilon \sim \frac{v_\lambda^3}{\lambda} \sim \lambda^{3r-1} \Longrightarrow r = \frac{1}{3} \Longrightarrow t \sim \lambda^{\frac{2}{3}}$$

This result indicates the time evolution of smaller scales of the perturbation, at which the structures of that scale are deformed.

With their hypotheses, Kolmogorov is placed in an ideal framework where the fluid within the inertial range recovers the symmetries of the Navier-Stokes equations lost in the turbulent transition, the energy injected from the macroscopic scales is transmitted without loss until to reach the Kolmogorov scale where the frictional forces represented by the viscosity dissipate the energy. Under these conditions a structure function $S_2(R)$ is postulated.

$S_2(R)$ measures the quadratic variations of the velocity in the longitudinal direction between two points separated by a distance $|\mathbf{R}| = R$, assuming that the fluid is self-similar by sufficiently high Reynolds numbers [1].

$$S_2(R) = \left\langle (\delta v\,(\boldsymbol{x}))^2 \right\rangle = \left\langle \left([\mathbf{v}(\mathbf{x}+\mathbf{R}) - \mathbf{v}\,(\mathbf{x})]\,\frac{\mathbf{R}}{R} \right)^2 \right\rangle$$

Since there can be no dependence on viscosity α must be $\frac{2}{3}$.

$$\left.\begin{array}{l} S_2(R) = C v_{\lambda_0}^2 (\frac{R}{\lambda_0})^\alpha \\ \frac{v_{\lambda_0}^2}{\lambda^{\frac{2}{3}}} = \left(\frac{v_{\lambda_0}}{\lambda_0^{\frac{1}{3}}}\right)^2 = \left(\varepsilon^{\frac{1}{3}}\right)^2 = \varepsilon^{\frac{2}{3}} \end{array}\right\} \rightarrow S_2(R) = C\varepsilon^{\frac{2}{3}} R^{\frac{2}{3}}$$

This result is known as Kolmogorov's law $\frac{2}{3}$ and has been experimentally validated.

In a general sense, the p-th order longitudinal structure function, for two points located at the positions $\boldsymbol{x}$ and $(\boldsymbol{x}+\mathbf{R})$ is given by

$$S_p(R) = \langle (\delta v\,(\boldsymbol{x}))^p \rangle = \left\langle \left([\mathbf{v}(\mathbf{x}+\mathbf{R}) - \mathbf{v}\,(\mathbf{x})] \frac{\mathbf{R}}{R} \right)^p \right\rangle \tag{4.2}$$

A generalization of Koomogorov's $2/3$ law is given by

$$S_p\,(R) = C_p \epsilon^{\frac{p}{3}} R^{\frac{p}{3}} \tag{4.3}$$

The universal nature of the structure function, and in particular the constant C postulated by Kolmogorov, was objected to by Landau and Lifshitz who postulated that the turbulent transition occurs when the system gradually gains degrees of freedom until it reaches a state that, despite being deterministic, is complex and difficult to deal with. The problem of the universality of the turbulence generation mechanism remains open pending a solid experimental verification.

4.3 Variation of β parameter

The following figure (FIG. 4.1) show the normalized energy spectra of 2000 particles in suspension in a fluid within a cubic lattice whose edge has 128 units, which corresponds to a concentration of $\phi = 0.06$, and $\beta = \frac{b_2}{b_1} = 1$. The curve is calculated from the $Fourier$ transform of the average over 4×10^6 iterations, performed in *Mare Nostrum Supercomputer* with $Ludwig$ code. The spectrum displays a plateau at small wavenumbers, consistently with theoretical predictions [44] for very dilute systems, followed by an algebraic decay, k^{-3}, which is a value in agreement also with the value obtained with the shell model, explained in the next chapter.

We show now a set of curves (FIG. 4.2) that correspond to values of values $\beta = \pm 1, \pm 10$ are the consequence of the combination $b_2 = \pm 1, \pm 0.1$ with $b_1 = 0.01$. For $\beta = \pm 10$ the energy spectrum is broader, which means that the total energy of the system is distributed on more scales, although it is still concentrated in the upper range. Compared to the case with $\beta = 1$, a lower incidence of the inverse cascade phenomenon is observed and therefore a significantly softer active

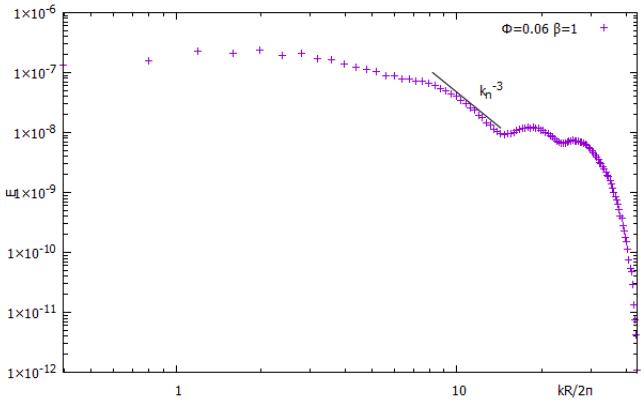

Figure 4.1: *Time averaged energy spectrum for* $\phi = 0.06$ *into a grid of size* $128 \times 128 \times 128$ *with* $\beta = 1$. *We can see a plateau at small wavenumbers followed by an algebraic decay,* k^{-3}.

turbulence is occurring: as higher orientation level of the system is, lower turbulence level for a given active particles self propelling velocity is produced. There are not differences between pullers and pushers. There is also a significant increase in the value of the local slope of the inertial range, propitiated by a more abrupt diffusivity.

In other words, the displacement difficulties produced by the low correlation of the particles orientation vectors strain the systems, favouring a powerful phenomenon of inverse cascade that accumulates most of the energy on the upper scales in form of internal energy. Fluids with a great correlation ($b_2 >> 0.01$) between suspension colloids fails to inject as much energy into the larger scales because movement is easier and dissipates the internal energy of the system in the form of kinetic energy.

Another example is found in the figure when comparing different beta values for phi=0.012. In this figure it is worth noting the severe change in shape as the absolute value of beta increases, the difference between pullers and pushers being much more marked for the higher value.

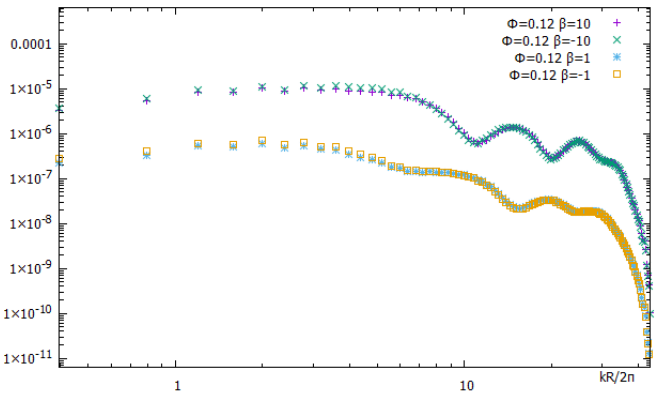

Figure 4.2: *Averaged energy spectrum for different β values ($b_1 = 0.01$ and $b_2 = \pm 0.01, \pm 0.1$). The energy spectrum is broader for $\beta = \pm 10$ and show a significant increase in the value of the local slope of the inertial range. There are not differences between pullers and pushers.*

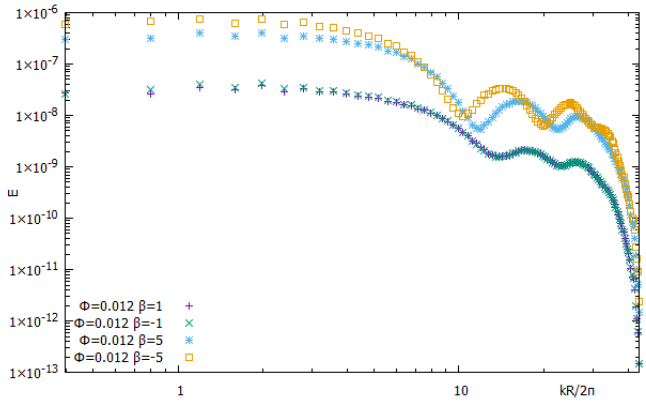

Figure 4.3: *Averaged energy spectrum for different β values ($b_1 = 0.01$ and $b_2 = \pm 0.01, \pm 0.05$). The energy spectrum presents a clear shape change for different values of b_2.There are differences between pullers and pushers.*

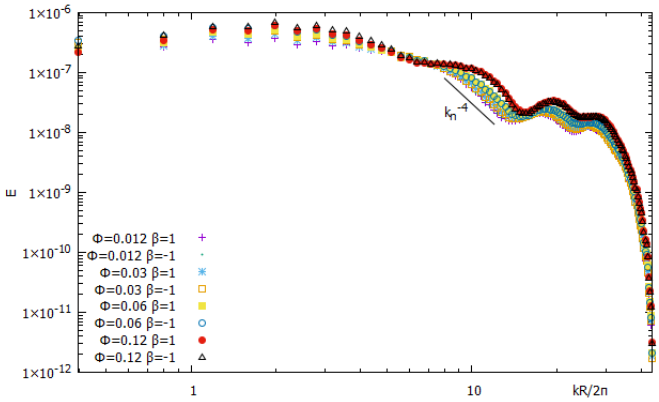

Figure 4.4: *Normalized averaged spectrum for different values of concentration, ϕ. $\beta = \pm 1$ corresponds to $b_1 = 0.01, b_2 = \pm 0.01$.There is a difference in the value of local slope but no significant topological changes are observed.*

4.4 Variation of concentration

The results obtained by calculating the normalized energy spectrum for different concentrations, ϕ, keeping the value $|\beta| = 1$ constant, for pullers and pushers, are shown in FIG. 4.4.

For different values of the concentration, ϕ , the spectrum do not significantly modify its shape so there is not a change in the energy distribution at different scales. However, there is a difference in the value of local slope, which reveal a change in the dynamic of the particles. As no significant topological changes are observed, no evidence is found that the decrease in concentration, at least in the numerical range studied, moderates or increases the inverse cascade phenomenon.

It is interesting to note that in relation to the previous chapter, the strong change in behaviour between pullers and pushers observed in terms of MSD and polar order is not reflected in a change in the shape of the energy spectrum. The energy distribution is therefore the same, which makes us think that the energy level is the same regardless of whether it manifests itself in the form of kinetic energy or not.

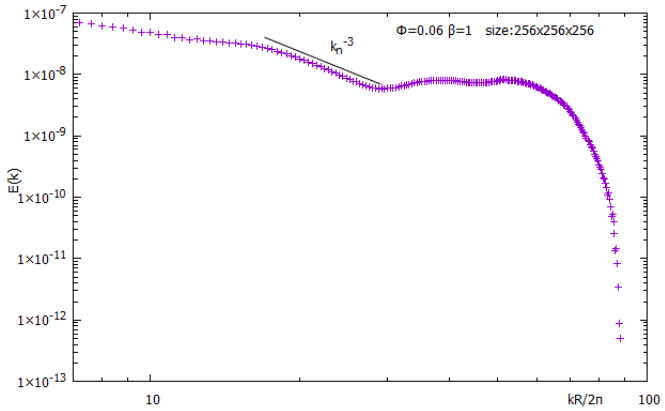

Figure 4.5: *Time average energy spectrum for* $\phi = 0.06$ *into a grid of size* $256 \times 256 \times 256$ *with* $\beta = 1$*. The value of local slope in the inertial range is the same as that observed for smaller systems.*

4.5 System size analysis

Next, we will analyse how the size of the grid affects the results (FIG. 4.5). For this, a simulation has been carried out in the Mare Nostrum Supercomputer with a grid of size $256 \times 256 \times 256$, a concentration of $\phi = 0.06$ and $\beta = 1$ ($b_1 = 0.01, b_2 = 0.01$). We run the simulation until 2×10^6 time steps ($TSTEP$). No significant changes are observed with respect to the first one case, where the size of the grid was smaller. The most notable fact is the value -3 in the local slope of the spectrum in the inertial range, which is obtained also for the smaller grid $128 \times 128 \times 128$, remain as theoretical framework predicted.

In Fig. 4.6 we report the energy spectrum of a numerical simulation in triperiodic cubic box of side $L = 512$ lattice points, with $N \approx 2.6 \times 10^5$ pushers of radius $R = 2.3$ lattice units (corresponding to a volume fraction of $\phi \approx 0.1$) and $\beta = -5$. The first squirming parameter is set to $b_1 = 1.5 \times 10^{-3}$ [65]. We observe the scaling $E(k) \sim k^{-3}$ in the inertial range.

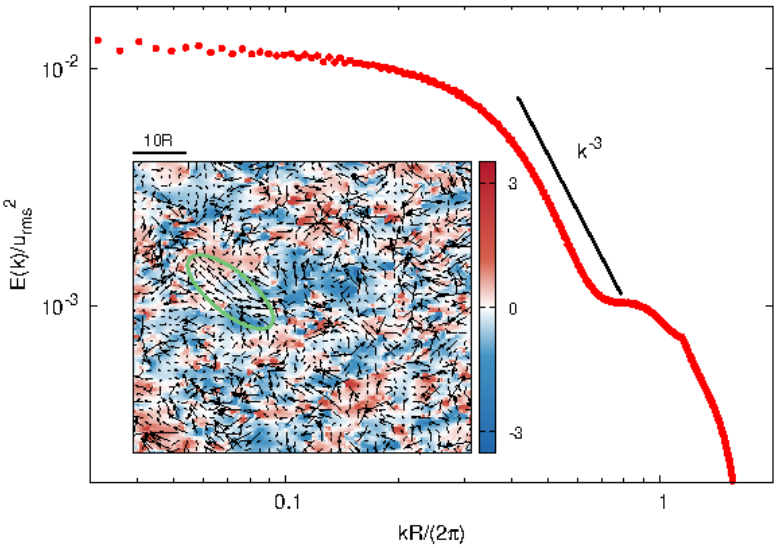

Figure 4.6: MAIN PANEL: Energy spectrum (time-averaged over the statistically stationary state) of the fluid velocity field, normalized by the mean square velocity u_{rms}^2, in a suspension of pushers ($\beta = -5$) at a volume fraction $\phi \approx 0.1$; the solid line indicates the scaling $E(k) \sim k^{-3}$. INSET: Snapshot of the velocity field in the plane $z = L/2$ from a simulation: the in-plane vectors (u_x, u_y) are depicted as arrows and the out-of-plane component u_z (rescaled by the characteristic swimming speed V_p) as a color map. Notice the size of correlated regions as compared to the microswimmer size $\sim R$; in particular, the occurrence of a *jet* extending on a scale of several particle radii is highlighted by the green ellipse.

4.6 Conclusions of the chapter

We showed that the energy spectrum develops decays with the power-law k^{-3} over a range of intermediate wavenumbers. It was posited that, given the lack of a *Richardson-Kolmogorov* energy cascade as in classical turbulence, the excitation of motion at large scales should be ascribed to the coupling between fluid velocity gradients and active particles orientation, i.e. to the flow alignment mechanism.

Through the energy spectrum, it is found that a low level of orientation in the suspended particles favours the appearance of the inverse cascade phenomenon, which is directly related to soft active turbulence. Higher levels of collective orientation lead to a more even distribution of energy across the scales. This fact is corroborated comparing the local slope and the shape of several energy spectrums performed for different b_2 values.

The decrease in concentration, ϕ, has no effect in this regard. We could speculate that although the proportion of energy that manifests itself kinetically with respect to that accumulated internally is clearly greater for pullers than for pushers, the energy distribution across the different scales is similar. In other words, the clear effect of increasing MSD and polar order shown in the previous chapter is not reflected in the energy spectrum.

We do not observe differences between pullers and pushers in any case.

CHAPTER

5

Shell-model

Shell-models are deterministic dynamical systems based on the discrete iteration of different modes of the same function, this highly repeated self-action aims to reproduce the essential features of complex continuous systems reducing the complexity of the full field equations. In no case does the shell-model try to model any physical reality, that is, it is not intended to be a mathematical description of a certain phenomenon or dynamics, but rather they offer the possibility to investigate the chaotic dynamics and multiscale correlations of turbulence with obvious computational advantages and, sometimes, even amenability of analytic treatment being a tool capable of producing universally applicable results. The great advantage of shell-models is their simplicity and their great versatility to introduce greater or lesser complexity into the equations, allowing the effect of each term or function added to the model to be quantified. In essence, they allow us to model the ingredients of the underlying fundamental physics shared by a given set of systems.

In this chapter, the characteristics of the classic shell-models (GOY-model and SABRA-model) will be explained. In this sense, a description of a novel model developed during the process of preparing this doctoral thesis will be made. We call this model SabrActive-model and it relates two fields: the velocity field and the orientation field. The interactions between both represent an attempt to reproduce

results in the field of active turbulence.

We will discuss, then, some results of simulations carried out with SabrActive-model, whose numerical and analytical study confirms the spectrum power-law observed in the previous simulations and reveals hints of a non-Gaussian, intermittent, physics of active turbulence. Direct numerical simulations and modelling also agree in pointing to a phenomenological picture whereby, in the absence of an energy cascade *à la Richardson* forbidden by the low Reynolds number regime, it is the coupling between fluid velocity gradients and particles orientation that gives rise to a multiscale dynamics.

5.1 Classical Shell-models

5.1.1 GOY-model

The basis of this shell model is found in Gledzer's article [22] (based on Obukhov's 1971 equations, published two years earlier to try to describe ocean mechanics) and in Yamada and Ohkitani's articles [23-25] proposing an improvement of the model using a complex variable. In fact, the name of the model includes the initials of the three authors. It is a turbulence shell model, which has a low chaotic attractor with which it shares statistical properties similar to real inertial turbulence.
The equations of a shell-model do not carry any of the geometrical information contained in the original system. The purpose of the GOY-model is not to justify the equation of the model with, for example, an asymptotic analysis but with the scaling exponents of the structure functions, $\xi^{NS}(p)$, that match the model and the experiments. The exponents of low-order functions reproduce the situation described by Kolmogorov in 1941. The structure functions follow the law *(4.3)*, in particular for the case $p = 2$ follow the law $2/3$ that in terms of shells can be expressed as [1]

$$E(k_n) = C\epsilon^{\frac{2}{3}} k_n^{-\frac{5}{3}} \tag{5.1}$$

On the other hand, the anomalous exponents, $\xi^{SM}(p)$, that determine the predicted deviation in Kolmogorov's theory and that give rise to the phenomenon known as intermittency [7], are found in the model. Following the power law predicted by the model for the energy spectrum and determining the approximate numerical values of the anomalous exponents are the two most commonly used checks to validate computational simulations of models of the Navier-Stokes equations. The approximation to these results is made from the calculation of the Lyapunov exponents to a phase space defined by the index j, which determines the Lyapunov vector, situating it in the spectrum of Fourier modes (expressed as components of the Lyapunov vector). In both 2D and 3D simulations there are clearly located peaks that indicate a form of correspondence between the two bases (FIG.5.2). A strong correspondence to the dissipative range and a weak correspondence to the inertial range are observed.

Describing the time evolution of complex variables, $u_n(t)$ (with $n = 1, 2, ..., N_s$), that can be thought of as a sort of Fourier amplitudes of velocity fluctuations over a length scale with associated wavenumber k_n, the general equations governing the process are a system that links each equation corresponding to a given shell with its predecessor and successor, G_n, and giving two conserved quadratic integrals that are physically identified by energy, E, and vorticity, Ω.

$$\left(\frac{d}{dt} + \nu k_n^2\right) u_n = iG_n[u] + f_n \tag{5.2}$$

$$E = \frac{1}{2}\sum u_n^2 \tag{5.3}$$

$$\Omega = \frac{1}{2}\sum k_n^2 u_n^2 \tag{5.4}$$

The complex variable u_n represents the temporal evolution of the variation of the velocity in different scales equispaced by a value λ that normally takes the value 2:

$$k_n = k_0 \lambda^n$$

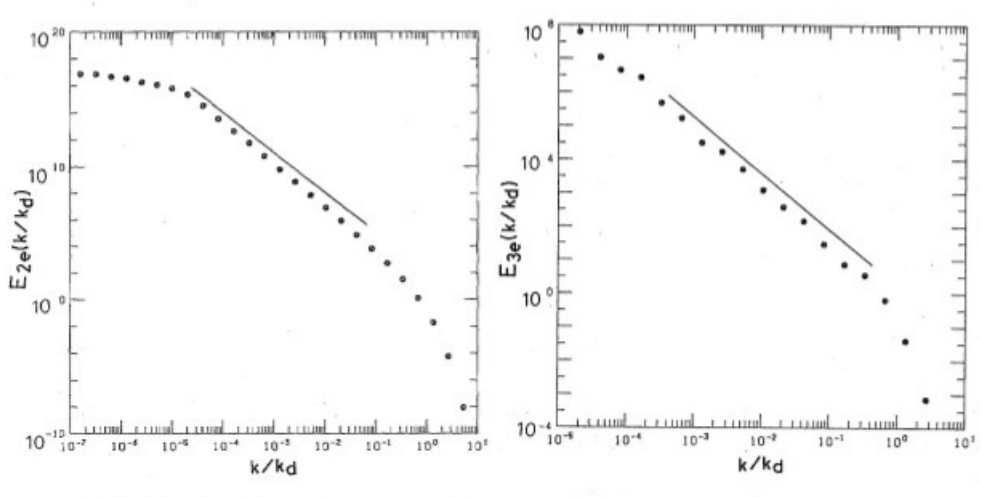

Figure 5.1: *Image from reference [24]. Inertial rang in the energy spectrum calculated by GOY-model*

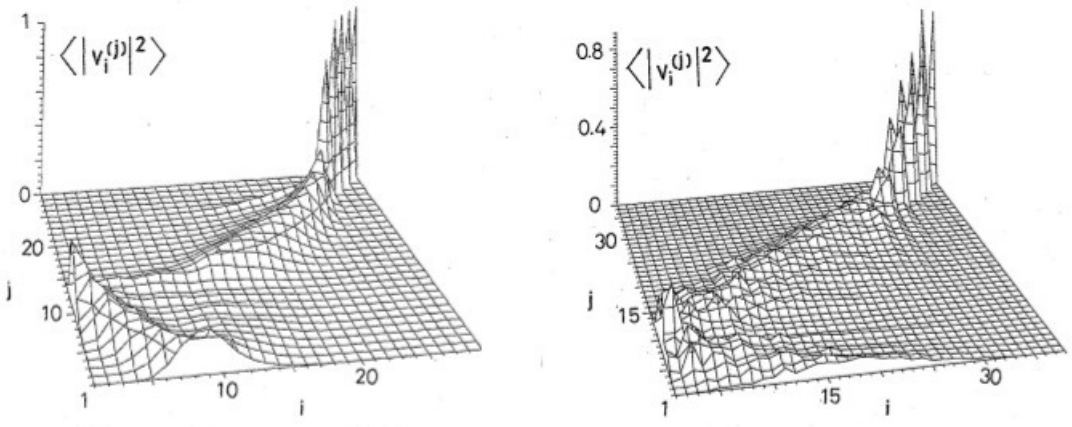

Figure 5.2: *Image from reference [24]. Lyapunov exponents located peaks as they were represented in the original article.*

This evolution is determined by the energy injected into the system, represented by the external force f_n which is usually nonzero only on the upper scale ($n \leq L_0$); by the degree of dissipation, related to the viscosity ν which begins to be effective below the Kolmogorov scale ($n \geq \lambda_0$); and by the interaction between the different scales, determined by the function $G[u]$ which is taken in the form:

$$G[u] = [ak_{n+1}u_{n+2}u_{n+1} + bk_n u_{n+1}u_{n-1} + ck_{n-1}u_{n-1}u_{n-2}]^* \tag{5.5}$$

5.1.2 SABRA-model

Subsequently to the works of Yamada, Gledzer and Ohkitani, other authors [34] introduce a modification in the GOY-model that affects the number of complex conjugate operators but not the fundamental properties of the model. This improved model is called SABRA-model and is given by the function

$$\phi[u] = ak_{n+1}u_{n+2}u^*_{n+1} + bk_n u_{n+1}u^*_{n-1} - ck_{n-1}u_{n-1}u_{n-2} \tag{5.6}$$

so SABRA-model will behave analogously to GOY-model in terms of scaling law. This statement is supported by the results of several numerical simulations [37] in which the clearest conclusion is a behaviour consistent with a direct cascade image for $a = 1, b = -2$ and $c = -1$ in a SABRA-model reproducing the results obtained with GOY-model in an equivalent situation.

Since second and third order structure functions are defined as a time average in the following way

$$S_2(k_n) = \langle u_n u^*_n \rangle \tag{5.7}$$

$$S_3(k_n) = Im\left\langle u_{n-1}u_n u^*_{n+1}\right\rangle \tag{5.8}$$

if the system is studied in inertial mode, this is $f_n = 0$ and $\nu = 0$, we get the expression

$$\frac{d}{dt}S_2(k_n) = ak_{n+1}\left|S_3(k_{n+1})\right| + bk_n\left|S_3(k_n)\right| - ck_{n-1}\left|S_3(k_{n-1})\right| \tag{5.9}$$

5.1.3 Energy flux equilibrium

The steady state $\frac{dE_n}{dt} = \frac{d}{dt}S_2(k_n) = 0$ can be expressed with the balance equation [34]:

$$C(k_n) = \frac{ak_{n+1}|S_3(k_{n+1})| + bk_n|S_3(k_n)| - \nu k_n^2 u_n}{ck_{n-1}|S_3(k_{n-1})|} = 1 \qquad (5.10)$$

This balance describes the turbulent phenomenon as a competition between the energy flow from the upper to the lower scales and the energy flow in the opposite direction. If $C(k_n) > 1$ then there is a net flow of energy to the lower scales (direct cascade). If $0 < C(k_n) < 1$ then there there is a net flow to the upper scales (inverse cascade).

In the above equation, in the inertial range the term with coefficient c is offset by the first two terms of the right member, since the viscosity is zero and f_n only acts on the upper scales, $n \leq L_0$. In the viscous range, that is, for scales below the Kolmogorov scale, $n \geq \lambda_0$, the term with coefficient c is offset by the term viscous, which acts as a cutoff, because the structure functions of order 3 of coefficients a and b go to zero quickly. Within the inertial regime (no input or loss of energy) the total energy of the system must be conserved and, therefore, the total variation of the energy must be zero:

$$\frac{dE}{dt} = \sum_n \frac{dE_n}{dt} = 0$$

Indeed, if we add the n equations 5.6 and group the terms with the same value of k, we obtain n terms of the form

$$(a + b - c)k_n|S_3(k_n)|$$

in order to guarantee this conservation law, it must comply with $a + b - c = 0$. It is also necessary to guarantee the stationary regime the condition of contour at the ends:

$$b_0 = b_N = c_0 = c_1 = a_{N-1} = a_N = 0.$$

The equilibrium constant $0 \leq C(k_n) \leq 1$ (5.10) can be interpreted as a flow of energy, $\Pi_E(k_n)$ between the scales $n-1$, n and $n+1$ [40]. Since $a+b-c=0$ is a general constraint of the SABRA model we consider $a=1, b=-\epsilon$ and $c=(1-\epsilon)$ with $0 \leq \epsilon \leq 1$, [33] without loss of generality, so

$$\begin{aligned} \mathit{\Pi}_E(k_n) \equiv (C(k_n)-1)\,|S_3(k_{n-1})|\,(1-\epsilon)\,k_{n-1} = \\ |S_3(k_{n+1})|\,k_{n+1} - \epsilon\,|S_3(k_n)|\,k_n - |S_3(k_{n-1})|\,(1-\epsilon)\,k_{n-1} \end{aligned} \tag{5.11}$$

$$\begin{aligned} \mathit{\Pi}_E(k_n) < 0 \Longrightarrow 0 < C(k_n) < 1 \Longrightarrow InverseCascade(IC) \\ \mathit{\Pi}_E(k_n) > 0 \Longrightarrow C(k_n) > 1 \Longrightarrow DirectCascade(DC) \end{aligned} \tag{5.12}$$

In this way, a model is developed for the N-S equations within the context of the SABRA-model

$$\frac{d}{dt}S_2(k_n) = \mathit{\Pi}_E(k_n) + p_n \tag{5.13}$$

$$\frac{d}{dt}C(k_n) = (1-\lambda)\phi_n^B - \lambda\phi_n^F - \gamma C(k_n) \tag{5.14}$$

SABRA-model equations are validated as a model that reflects the basic characteristics of the turbulent regime. The function ϕ_n^F represents a forward energy flow (Direct Cascade) and the function ϕ_n^B represents a backward flow (Inverse Cascade). The coefficients λ and $(1-\lambda)$ come from an idea proposed in [18]. If $\lambda = 1$ a regime of direct cascade is obtained and if $\lambda = 0$ a cascade inverse regime, any other value of $\lambda\ \epsilon\ [0,1]$ gives a mixed dynamics. $-\gamma C(k_n)$ is a self-advection term determined by a relaxation time of the γ^{-1} system.

5.2 SabrActive-model

5.2.1 Model equations

The generalized version of the SABRA-model, which has been developed in this doctoral thesis, is based on relating two fields (instead of one as usual) through the function

$$\begin{aligned}\phi_n^{(b)}[u,v] = k_{n+1}\left[(1-b)\,u_{n+2}v_{n+1}^* + (2+b)\,u_{n+1}^* v_{n+2}\right] + \\ k_n\left[(2b+1)\,u_{n-1}^* v_{n+1} - (1-b)\,u_{n+1}v_{n-1}^*\right] + \\ k_{n-1}\left[(2+b)\,u_{n-1}v_{n-2} + (2b+1)\,u_{n-2}v_{n-1}\right]\end{aligned} \tag{5.15}$$

This function $\phi_n^{(b)}[u,v]$ [35][38] is a generalization of the ones seen above to quantify the nonlinear terms in the equations. If there is only one field present, $u = v$, the above equation returns to the usual SABRA-model form with the parameterization $a = 3, b = 3b, c = -3(b+1)$

$$\phi_n^{(b)}[u,u] = 3k_{n+1}u_{n+2}u_{n+1}^* + 3bk_n u_{n+1}u_{n-1}^* + 3(b+1)k_{n-1}u_{n-1}u_{n-2} \tag{5.16}$$

From references [46-50] we take the equations of motion that are appropriate to define the situation that interests us. Obviously they are not the only valid system of equations, there are other options in the literature that, although they share the general lines and approaches, refer to other theoretical and experimental situations [12][26-31].

$$\rho\left(\partial_t\mathbf{u} + \mathbf{u}\nabla\right)\mathbf{u} = -\nabla p + \eta\nabla^2\mathbf{u} + \nabla\sigma^{(a)} \tag{5.17}$$

$$\partial_t\mathbf{P} + \left(\mathbf{u} + \omega\mathbf{P}\right)\nabla\mathbf{P} = \mathbf{\Omega P} - \Gamma\mathbf{P} + D\nabla^2\mathbf{P} \tag{5.18}$$

The active stress, $\sigma^{(a)}$, appearing in the Navier-Stokes equation (5.17) is given by $\sigma(a)_{ij} = \xi P_i P_j$ [47], where the parameter ξ is proportional to the swimmers volume fraction and to the amplitude of the generated stress and, therefore, quantifies in some sense the level of activity. Ω denotes the antisymmetric part of the velocity gradient tensor, $\Omega_{ij} = \frac{1}{2}(\partial_i u_j - \partial_j u_i)$ and η and D are the fluid dynamic viscosity and the orientation field diffusion coefficient, respectively. Except for the term $\omega(P\nabla)P$, Eqs. (5.17-5.18) closely resemble the Oldroyd-B equations for the polymer conformation in vectorial form.

From the general form of the equations, a shell model must be formulated for which the appropriate terms must be chosen. Each term can refer to the interaction

or self-action of the two fields involved and can generate an energy flow in two directions (towards large values of k or towards small values) Different variations will presumably produce different results and, in fact, the study of them is a line of research of interest for the future. Superindex ϵ may represent a backward and forward energy transfer respectively modulated by the coefficients ω. Different theoretical and phenomenological considerations, several conjectures and various previous tests eventually lead to the following structure for the sought shell model:

$$\frac{du_n}{dt} = \frac{i}{3}\phi_n^{(\epsilon)}(u,u) - \gamma_u(k_n)u_n + f_n^{(a)} \tag{5.19}$$

$$\frac{dP_n}{dt} = \frac{i}{3}\phi_n^{(\epsilon)}(u,P) + \frac{i\omega}{3}\phi_n^{(\epsilon)}(P,P) - \frac{i}{3}\phi_n^{(\epsilon)}(P,u) - \gamma_P(k_n)P_n - \Gamma P_n \tag{5.20}$$

The dynamic equations of our shell model have to be similar to GOY-model equations (5.2) but also try to reproduce, or at least capture the essence, of the (5.17-5.18) equations since it combines the self-action of the particles, $\mathbf{P}$, with the movement of a fluid that surrounds and transports them, $\mathbf{u}$. Therefore the equations above can be related to the study of active matter and this is the reason why we refer to this model as *SabrActive-model* for active turbulence modelling.

From a first formal inspection of the equations proposed by the model, the following characteristics can be deduced:

- The set of wave numbers is taken to be $k_n = k_0 2^n$
- u_n represents the velocity field relative to the general motion of the (incompresible) fluid.
- P_n represents an order parameter quantifying the degree of local orientation. It can be caused by a suspension of active particles witch intrinsic swimming director could cause changes in the topology and overall functioning of the fluid.
- We enforce a zero Reynolds number regime and do not account for non-linear momentum transfer, setting $\Phi_n^{(\varepsilon)}(u,u) = 0 \quad \forall n$ in (5.19).

- $\gamma_P = \nu_{u,P} k_n^2 + \mu_{u,P} k_n^{-4}$ where $\nu_{u,P}$ are the actual viscosity and diffusion coefficient, acting at small scales (large wavenumbers), whereas $\mu_{u,P}$ are large scale drag coefficients, mimicking friction with the boundaries.

- The velocity of active fluids is governed by a scale-matched balance of active forcing and viscous dissipation [42]; accordingly, the divergence of the active stress $\sigma^{(a)}$ is described by a *local-in-scale* (or, equivalently, in wavenumber) force in the shell model, $\nabla \cdot \sigma^{(a)} \to f_n^{(a)} = i k_n \zeta P_n^2$.

- Flow alignment, whereby velocity gradients are coupled to microswimmers orientations [46, 48, 49], provides a different mechanism, related to the emergence of collective motion (involving P), that excite multiple scales in the fluid, generating turbulence. Consistently, we assume that the rotation term, $P\nabla u$, is responsible for the upwards transfer, and set $\varepsilon = \varepsilon_b < \varepsilon_c$ in the operator $\Phi_n^{(\varepsilon)}(P, u)$ in (5.20). Moreover, the advective, $u\nabla P$, and self-advective, $P\nabla P$, terms have mixing properties that tend to disrupt spatial orientational coherence and, therefore, to transfer downwards; we set, then, $\varepsilon = \varepsilon_f > \varepsilon_c$ in the operators $\Phi_n^{(\varepsilon)}(u, P)$ and $\Phi_n^{(\varepsilon)}(P, P)$ in (5.20). Interpreting ε_c as a critical value in the continuous variation of the balance of flows in a similar way to the description of the equation 5.10.

- In equation (5.18) the term ΓP_n is related to diffusion and is therefore expected to be only significant for large values of n in a net straight cascade regime.

- These equations model a competition between the two energy cascades. It is known that there are channels where the two flows are present (direct or inverse) but there are also situations that allow a clear action in one direction in both directions.

- In the literature you can find publications that expose models similar to the *SabrActive-model* such as the reduction of the viscosity of a solution with the addition of polymers [39]

These mechanisms lead eventually to the *SabrActive* shell model

$$\dot{u}_n = -\gamma_u(k_n)u_n + i\zeta k_n P_n^2$$
$$\dot{P}_n = \frac{i}{3}\Phi_n^{(\varepsilon_f)}(u,P) + \frac{i}{3}w\Phi_n^{(\varepsilon_f)}(P,P) - \frac{i}{3}\Phi_n^{(\varepsilon_b)}(P,u) - \gamma_P(k_n)P_n - \Gamma P_n + \delta_{n,n_B}|P_n|^{-1}P_nP_B. \tag{5.21}$$

5.2.2 Validation of the phenomenological assumptions from the numerics

We have seen in the previous section how the development of a shell model relies crucially on the knowledge of the transfer of dynamical fluctuations of a field across scales. Lacking a Richardson cascade, we had to conjecture the direction of fluxes in spectral space of non-linear terms involving the orientation and velocity field on the basis of phenomenological arguments. Here, we want to justify these conjectures, benchmarking them against direct numerical simulations. Since our numerical method couples a Lagrangian dynamics for colloids with a Eulerian description of the fluid, though, first we need a procedure that maps the particle positions and orientations to the field $\mathbf{P}$. To this aim we divide ideally the computational box in $(L/\Delta)^3$ subdomains $\mathcal{I}_\Delta^{(m)} = \{\mathbf{x} \in L^3 : |x_i - X_i^{(m)}| < \Delta/2,\, i = 1,2,3\}$ and introduce the following representation of $\mathbf{P}$

$$\mathbf{P}_\Delta(\mathbf{X}^{(m)},t) = \frac{1}{N_\Delta^{(m)}(t)} \sum_i^{N_\Delta^{(m)}(t)} \hat{e}_i(t), \tag{5.22}$$

on the lattice defined by the set of points $\mathbf{X}_m = \Delta/2 + \mathbf{m}\Delta$, with $\mathbf{m} = (m_x, m_y, m_z)$ a vector of integers ranging from 0 to $L/\Delta - 1$. The sum in (5.22) runs over the $N_\Delta^{(m)}$ particles contained in $\mathcal{I}_\Delta^{(m)}$ at time t. Analogously we construct a velocity field that lives on the coarse lattice as:

$$\mathbf{u}_\Delta(\mathbf{X}_m,t) = \frac{1}{\Delta^3} \sum_{\mathbf{x}\in\mathcal{I}_\Delta^{(m)}} \mathbf{u}(\mathbf{x},t). \tag{5.23}$$

At this point by projecting the second of Eqs. (5.19, 5.20), with $\mathbf{u}$ and $\mathbf{P}$ replaced by $\mathbf{u}_\Delta$ and $\mathbf{P}_\Delta$, onto the Fourier mode $\mathbf{k}$, multiplying both sides by $\tilde{\mathbf{P}}_\Delta^*$ (the complex

conjugate of the Fourier transform of $\mathbf{P}_\Delta$), averaging over shells of radius k and summing with the complex conjugate equation, we get:

$$(\partial_t + \Gamma + Dk^2)\mathcal{P}_\Delta = \mathcal{F}_{\text{adv}} + \mathcal{F}_{\text{self}} + \mathcal{F}_{\text{rot}}, \tag{5.24}$$

where $\mathcal{P}(k,t) = \langle|\tilde{\mathbf{P}}_\Delta|^2\rangle$. The terms on the right hand side read as follows:

$$\begin{aligned}
\mathcal{F}_{\text{adv}}(k,t) &= -\langle\Big(\tilde{\mathbf{P}}^*_\Delta(\mathbf{k},t)\cdot\mathbf{J}_{\text{uP}}(\mathbf{k},t)\Big)\rangle + \text{c.c.} \\
\mathcal{F}_{\text{self}}(k,t) &= -\langle\Big(\tilde{\mathbf{P}}^*_\Delta(\mathbf{k},t)\cdot\mathbf{J}_{\text{PP}}(\mathbf{k},t)\Big)\rangle + \text{c.c.} \\
\mathcal{F}_{\text{rot}}(k,t) &= \langle\Big(\tilde{\mathbf{P}}^*_\Delta(\mathbf{k},t)\cdot\mathcal{R}(\mathbf{k},t)\Big)\rangle + \text{c.c.}
\end{aligned} \tag{5.25}$$

where $\mathbf{J}_{\text{uP}}(\mathbf{k},t)$, $\mathbf{J}_{\text{PP}}(\mathbf{k},t)$ and $\mathcal{R}(\mathbf{k},t)$ are the Fourier transforms of the non-linear terms of the orientation field equation, namely $\mathbf{u}_\Delta\cdot\nabla\mathbf{P}_\Delta$, $w\mathbf{P}_\Delta\cdot\mathbf{P}_\Delta$ and $\mathbf{\Omega}_\Delta\cdot\mathbf{P}_\Delta$, respectively, and "c.c." stands for the complex conjugate terms. Eqs. (5.25) are fluxes across k-shells in spectral space and whether a direct or inverse cascade of magnitude of orientation, depending on their sign, takes place. We measured them in then numerical simulations and the results, averaged in time over the statistically stationary state are plotted in Fig. 5.3. Although the coarse-graining procedure reduced the range of accessible scales, a clear qualitative difference appears: while $\mathcal{F}_{\text{adv}}$ and $\mathcal{F}_{\text{self}}$ (A and B panels) are negative at intermediate and large wavenumbers, signalling that they transfer orientation fluctuations towards small scales (i.e. they tend to disrupt coherence), the rotational spectral flux $\mathcal{F}_{\text{rot}}$ (C panel) is positive (and in magnitude larger than the previous two), therefore confirming our phenomenological conjecture that it is the term responsible for the upward cascade that eventually pumps energy into the large scales.

5.2.3 Code description

The code evolves iteratively through the time step, T, parameter. The ultimate goal is to obtain convergent values for the fields, $U[n]$ and $B[n]$. These fields have a complex vectorial character, each of its components being the value of the field on a given scale, denoted by the parameter n, and showing separately the real, $.R$, and imaginary, $.I$ components. There are three relevant functions in this code:

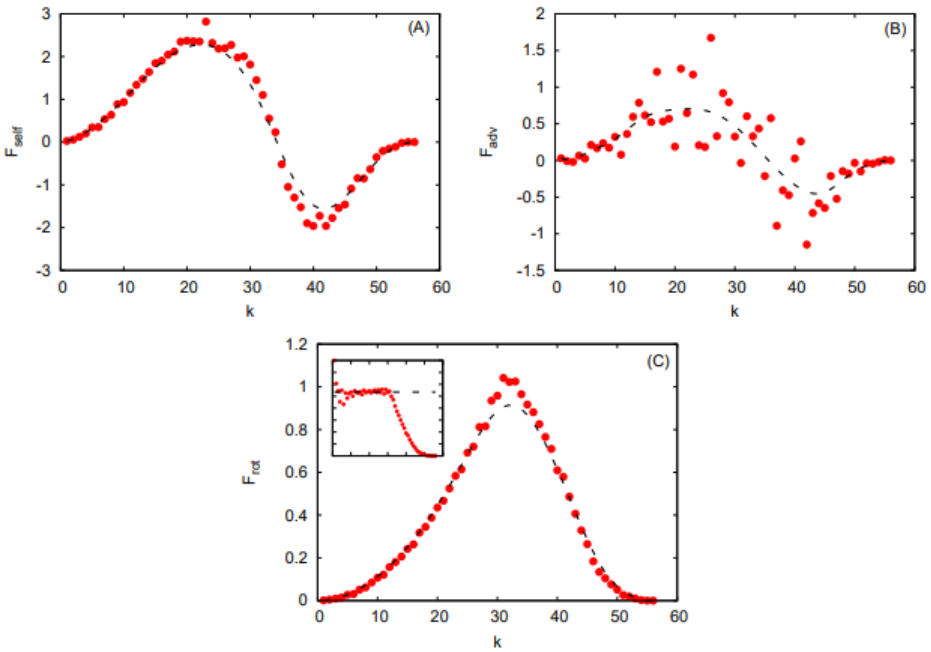

Figure 5.3: Spectral fluxes, Eq. (5.25), measured from the numerical simulations (time-averaged over the statistically stationary state): $\mathcal{F}_{\text{self}}$ (A), $\mathcal{F}_{\text{adv}}$ (B) and $\mathcal{F}_{\text{rot}}$ (C); the dashed lines depict a spline interpolation to the data. In the inset of panel (C) the flux per unit area (in spectral space), $k^{-2}\mathcal{F}_{\text{rot}}$ is shown, highlighting the presence of constant flux range of scales.

- The ϕ function, located at the beginning of the code, is the function of interaction between the U and B fields at N different scales. This is a generalization of the SABRA model, which should be recovered when U = B as we explained in the previous section. In fact, for a proper choice of the parameter b, the function ϕ would coincide with the one used in the classic SABRA-model.

- The functions U [n] and B [n] calculate the value of the n components of each field in each iteration. To do this, an iteration model composed of the value of the field in each iteration and its time derivatives in the present and previous iteration, is used. The recurring equation is of the fourth-order Runge-Kutta method.

- The equations of the model that we are studying relate the time derivative of the fields B [n] and U [n] to the other parameters of the model. In these equations lies the physics of the system. The theory predicts a large-scale region, an inertial range, and a dissipative region. This physical aspect is clearly imposed in the code by dividing the N scales into three levels. There is an initial level, corresponding to the first two scales, where the equations of the model are truncated and only the terms related to energy injection and large-scale drag are present. Then an intermediate level where all the terms of the model equations (5.21) are present. And a final level, corresponding to the last two scales, where only the dissipative terms are found.

In each iteration with certain values of $U[n;t]$ and $B[n;t]$ the function ϕ, which mixes the fields at different scales, is calculated. From the values of ϕ, $U[n;t]$ and $B[n;t]$ obtained, the time derivative of the fields is calculated through the equations of the model by certain values of the parameters. The value of the fields, at the different scales, is then calculated for the next iteration, $U[n;t+1]$ and $B[n;t+1]$. To get $U[n;t] = U[n;t+1]$ and/or $B[n;t] = B[n;t+1]$ the corresponding time derivatives must be zero (stationary state) and this happens for null value of the function ϕ. It is possible to run the code in no-active mode, $B[n] = 0$.

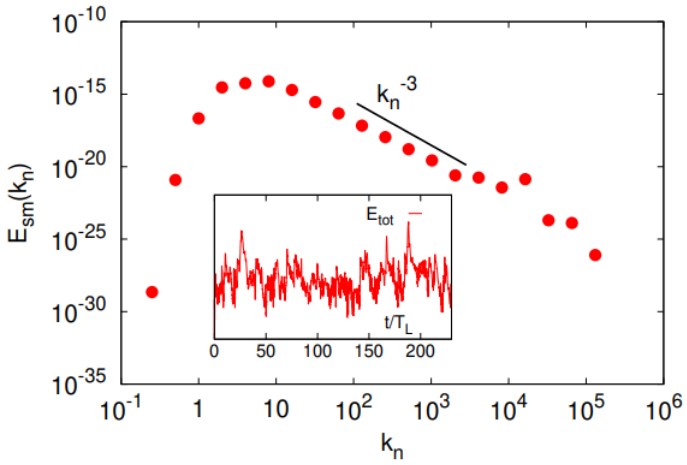

Figure 5.4: *MAIN PANEL: Time-averaged (over the steady state) energy spectrum from the simulation of the shell model for active turbulence, Eq. (5.21). INSET: Total energy,* $E_{tot}(t) = \sum_n |u_n|^2$ *vs time in units of integral scale characteristic time* $T_L = (k_{max} u_{rms})^{-1}$ *(*k_{max} *location of spectrum maximum and* $u_{rms} = \left(\sum |u_n|^2\right)^{\frac{1}{2}}$ *)*

5.3 Energy Spectrum

We integrated the system with $Ns = 20$ shells by means of a fourth-order Runge-Kutta scheme for $T = 6 \times 10^{11}$ time steps (with integration step $\delta t = 10^{-4}$). The following numerical values are used for the parameters:

$$k_0 = 2^{-4}, \varepsilon_f = -0.4, \varepsilon_b = -1.8, \nu_u = 10^{-6}, \mu_u = 10^{-10}, \zeta = 1.25 \times 10^{-2},$$
$$w = 1.25 \times 10^{-2}, \nu_P = 8.5 \times 10^{-13}, \mu_P = 10^{-10}, \Gamma = 10^{-6},$$
$$P_B = 5 \times 10^{-11}(1+i), n_B = N_s - 1$$

We plot the time average energy spectrum in the statistically stationary state. FIG. 5.4 shows that the energy spectrum develops decays with the power-law k^{-3} over a range of intermediate wave numbers, as we have seen before in chapter 4 for direct numerical simulations.

$$E_{sm}(kn) = \left\langle \frac{|u_n|^2}{k_n} \right\rangle \sim k_n^{-3} \tag{5.26}$$

It is possible to derive the power law decay of the energy spectrum, $E(k) \sim k^{-3}$, from the shell model. The evolution of the orientation magnitude, $|P_n|^2$, is

obtained multiplying the second of Eqs. (5.21) by P_n^* and the complex conjugate by P_n and summing the two, and reads

$$\partial_t |P_n|^2 \approx P_n^* \Phi_n^{(\varepsilon_b)}(P,u) + P_n (\Phi_n^{(\varepsilon_b)}(P,u))^* - \Gamma |P_n|^2 - \gamma(k_n)|P_n|^2, \qquad (5.27)$$

where the advective and self-advecting terms are neglected, consistent with the DNS results, see Fig. 5.3. Assuming statistical stationarity and focusing on intermediate k_n, where the flux dominates over dissipation (i.e. we look at the generalized inertial range), we see immediately that, dimensionally, $kuP^2 \sim$ cte whence,

$$P \sim k^{-1/2} u^{-1/2}. \qquad (5.28)$$

From the first of Eqs. (5.21) we get analogously that $k^2 u^2 \sim kuP^2$, whence

$$u \sim k^{-1} P^2. \qquad (5.29)$$

Plugging Eq. (5.28) into Eq. (5.29) yields $u_n \sim k_n^{-1}$, therefore the energy spectrum, $k_n^{-1}|u_n|^2$, should indeed behave as

$$E_{\text{sm}}(k_n) \sim k_n^{-3}. \qquad (5.30)$$

5.4 Statistical properties

To provide a further insight on the statistical properties of the *SabrActive-model*, we measure the PDFs of velocity variables u_n; representing fluctuations on a length scale $\sim k_n^{-1}$, they are the shell model counterpart of the velocity increments PDFs in the direct numerical simulations.

In Fig. 5.5 we plot the properly normalized PDFs of the real part of the shell velocity variable, $u_n^R = Re(u_n)$ (divided by its root mean square value, σ_n), with $n = 10$, $n = 12$ and $n = 19$.

For n = 19, corresponding to the smallest scales (interpretable with approximately that of a microswimmer), the data lie on a Gaussian (dashed line). At smaller n (larger scales, falling within the generalized inertial range), the PDFs maintain a Gaussian core, but the emergence of power-law tails at large u_n^R ($\geq 4\sigma_n$) can be appreciated (solid lines).

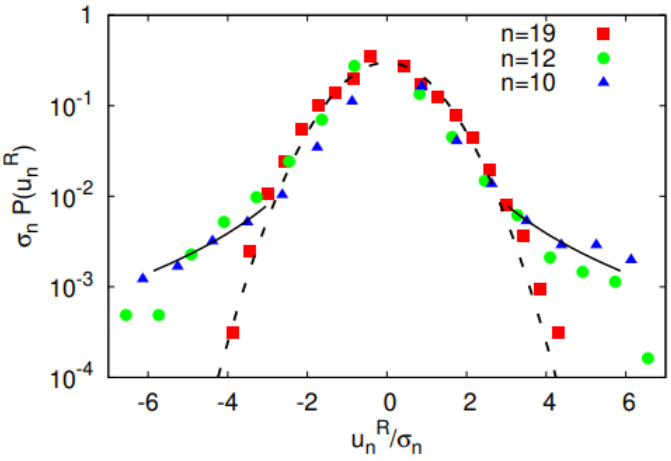

Figure 5.5: *PDFs of the real part of the shell model velocity variables (in units of their root mean square values, σ_n) with three different shell indices, corresponding to length scales within the generalized inertial range ($n = 10$ and $n = 12$) and down to the microswimmer scale ($n = 19$). The dashed line depicts the Gaussian probability density function with zero mean and standard deviation $\sigma = 1.5$, whereas the solid lines highlight power law tails of the form $\sim |u_n^R|^{-\alpha}$ with $\alpha = 2.5$*

5.5 Conclusions of the chapter

We have presented a massive computational study aimed at revealing the presence of active turbulence in diluted suspensions of finite size squirmers. We showed that the energy spectrum develops decays with the power-law k^{-3} over a range of intermediate wavenumbers. It was posited that, given the lack of a Richardson-Kolmogorov energy cascade as in classical turbulence, the excitation of motion at large scales should be ascribed to the coupling between fluid velocity gradients and particle orientation, i.e. to the flow alignment mechanism. Based on this picture and on phenomenological arguments, we developed a reduce order dynamical deterministic model (or shell model) of active turbulence, dubbed *SabrActive-model*. Numerical simulations and theoretical analysis of the model confirmed the k^{-3} scaling of the spectrum.

The introduction of this new model pushes forward the reach of quantitative tests of how actually "turbulent" is active turbulence, allowing to measure, e.g., Lyapunov exponents, higher order structure functions, multiscale statistics, etc, on "physically" much longer runs. A flavour of this capability can be grasped in the observation of intermittency in the PDFs of shell model velocity variables. Investigating the dynamical and statistical properties of the model and the sensitivity of the system response to changes in the control parameters (for instance, the onset of active turbulence at changing the activity parameter), as well as exploring a wider region of the volume-fraction/squirming-parameters space in direct numerical simulations are foreseen as natural follow-ups of the present work.

The detection of intermittency signatures in the shell model simulations is intriguing and should motivate further computational studies as well as dedicated experiments.

CHAPTER

6

Conclusions and perspectives

6.1 Summary of results

In this doctoral thesis a study has been made on the active matter, specifically on the semi-diluted suspensions of microswimmers. The work has been structured in five chapters. After a brief introduction, the results and methodology of a set of computational simulations have been described and, finally, these results have been compared with other simulations performed with a code that implements a shell model that we propose in the last chapter.

The first chapter presents the basic elements for describing the active matter. Some careful definitions are made and the type of particles that will be used in the simulations is selected, categorizing it and classifying it within all the possible ones in the body of the theory. A summary of the most relevant aspects of the theoretical framework that dominates the interactions and dynamic evolutions of active systems is also given.

The second chapter is based on the explanation of the Lattice-Boltzmann method (LBM) as an essential tool to carry out computational simulations. The movement mechanism of the particle model used is also explained, as well as its relationship

with the environment.

The third chapter presents results obtained with simulations performed with *Ludwig code* (LBM) varying the quotient between the self-driven velocity, b_1 and the level of orientation of the particles, b_2. It is seen that the variation of the concentration, ϕ causes a very significant increase of the mean squared displacement, MSD, by an orientation in the direction of the speed of self-conduction, such is for pullers ($\beta = \frac{b_2}{b_1} > 0$).
This same chapter shows how the increase in MSD is linked to a strong growth in the polar order of the system, P_∞. It is hypothesized that under these parametric circumstances the system relaxes by transforming internal energy into movement through an overordering of particles, encouraging them to flow without colliding with each other while being dragged by the fluid in which they are suspended.

In the fourth chapter, the energy spectrum calculated from the data produced by the same simulations as in the previous chapter have been studied. Each energy spectrum, properly normalized, represents the distribution of the energy of the particles in various Fourier modes that represent the scales of the system. According to theories for inertial turbulence, spectrum should typically consist of three parts. The lower k order scales, those related to larger interaction distances, usually accommodate the energy injection forces of the system and can be defined as macroscales where the whole of the fluid is considered as a whole or almost as a whole. Next, we can expect to observe an inertial range of scales whose scaling law can be predicted. It is therefore a linear variation on a logarithmic scale whose slope remains constant in this set of intermediate scales that one can refer to as a mesoscale. Finally, the logarithmic scale spectrum decays sharply, indicating the beginning of the set of microscales in which energy dissipation takes place.
There is a flow of energy from the upper scales ($k \sim 0$) to the lower scales called direct cascades, likewise there is also the inverse cascade, that is, the flow of energy in the opposite direction. Both energy currents are in a competitive regime. The system can evolve in a relaxed way, favouring the movement of the particles in a self-conducted way, or on the contrary, the level of interaction can be greater, shortening the average distance that a particle can travel in the suspension. Going

from one situation to the other, depends largely on measure of the polar order of the system. When there is a great correlation between the particles in terms of orientation, the system disperses the energy in the form of kinetic energy.
Our simulations reproduce the parts of the spectrum described by the theory and even fit the same local slope that they predict.
The clearest case is that of pullers with a low concentration, being of special interest the fact that the behaviour of pullers and pushers is clearly different, demonstrating a different physical behaviour in the relationship of the particle with the fluid depending on whether the orientation and velocity vectors on the particles are parallel or antiparallel. However, this behaviour that is clearly shown in the results of the third section of this doctoral thesis is not reflected in the results obtained for the energy spectrum, which makes us think that in the spectrum it is not possible to distinguish the part of the energy total that is invested in kinetic form of the part that accumulates internally.

In the fifth chapter are exposed the advantages, at the computational and conceptual level, of using a shell model to reproduce asymptotic properties of the type of systems to which this work refers. After describing the structure of classical shell models, *SabrActive-model* is described, which is an original generalization of *SABRA-model*. It has been studied and tested for the first time in this doctoral thesis. The results generated by the simulations with this code are compatible with the results obtained in the previous chapters as well as the theoretical framework.

6.2 Perspectives

- We hope that with the results presented in this doctoral thesis, *SabrActive-model* would be a model accepted which would allow will our group and other researchers to continue exploring the processes that regulate active systems, both at a parametric and dynamic level.

- The study initiated with this work should continue with the search for structures and groups formed intrinsically by the system as clusters or flocks.

- Intermittency is associated with rare events, whose statistical incidence to be appreciated needs, therefore, long observation times. The detection of intermittency signatures in the shell model simulations is intriguing and should motivate further computational studies as well as dedicated experiments.

- The introduction of this new shell model, *SabrActive*, pushes forward the reach of quantitative tests of how actually turbulent is active turbulence, allowing to measure, on much longer runs, Lyapunov exponents, higher order structure functions, multiscale statistics, etc.

- It would also be of great interest to add new terms to the *SabrActive* equations and study their impact on the results both in microswimmers suspensions and in other types of active systems.

- Investigating the dynamical and statistical properties of the model and the sensitivity of the system response to changes in the control parameters as well as exploring a wider region of the volume-fraction/squirming-parameters space in direct numerical simulations are foreseen as natural follow-ups of the present work.

- In short, our intention behind this work is to delve into the results obtained, generalize the application of the shell model described in this doctoral thesis and apply it to other areas of active matter.

If I may adopt a very general (and somewhat romantic) view of the subject of this thesis to finish it, I would say that all researchers who, in one way or another, delve into the mystery of active matter do so with the intention to understand how the phenomenon of self-organization occurs in very disparate systems that spontaneously and, apparently, stochastically manage to create structures that are so easy to recognize and so difficult to explain. The intuition that there is a fundamental and universal law that organizes matter and serves as a link between complex microscopic interactions and deterministic macroscopic reality is the big question that we all want to answer. This has been my main motivation to carry out this work and it is my main objective to continue researching.

CHAPTER

7

Resumen en castellano

Esta tesis doctoral trata del estudio de la materia activa, en particular de la dinámica de los micronadadores en suspensión semidiluida. Queremos explorar las capacidades de los ingredientes físicos básicos necesarios para generar estructuras emergentes en escalas mucho mayores que las de los agentes individuales. Se han realizado varias simulaciones usando dos software: código Ludwig (LBM) y *SabrActive-model* (modelo shell). El objetivo es mejorar la comprensión del fenómeno mediante el estudio de la transmisión de energía a través de las diferentes escalas que, característicamente, se dan con la aparición de movimientos correlacionados. La turbulencia activa suave es la parametrización óptima del modelo para poder estudiar la complejidad del problema en el momento en que se presenta. Para tal fin se estudia el desplazamiento cuadrático medio, el espectro de energía y la evolución del orden polar del sistema.

GOY-model reproduce aspectos de la turbulencia hidrodinámica a través de una modelización del sistema como una superposición de campos de velocidad complejos a diferentes escalas. A partir de modelos de capas más actuales y generales, conocidos como variaciones de *SABRA-model* hemos realizado simulaciones con un código original tipo *SABRA-model* generalizado a donde se hace interaccionar dos campos a través de diferentes escalas. Este modelo original, al que llamamos

SabrActive-model, reproduce resultados experimentales además de ser congruente con teorías consolidadas y aceptadas por la comunidad científica en el ámbito de Active Matter. En este sentido se han realizado simulaciones producidas por *Ludwig* que es un *open code*, basado en el método *Lattice-Boltzmann*, utilizado para realizar simulaciones de fluidos complejos en tres dimensiones a través de un conjunto de rutinas y comunicaciones. Con este código es posible configurar múltiples modelos con distintos valores de energía libre y otros parámetros. Se trata de un código especialmente interesante porque dada la relativa simplicidad de ejecución en relación con la potencia de simulación es ideal para poder extraer conclusiones físicas sin tener que enfrentarse a una complicada situación de programación. *Ludwig* se estructura como una biblioteca de modelos preconfigurados sobre los que se puede incidir a nivel paramétrico a través de un *input file*. La física subyacente se encuentra dentro del marco de la teoría *active nematics* y el programa permite crear condiciones periódicas de fronteras, interacción entre coloides en suspensión, cristales líquidos (utilizando las ecuaciones de *Landau-de Gennes*) y fluidos binarios. Todas las simulaciones se han llevado a cabo en el *cluster Albeniz* de la Facultad de Física en la Universidad de Barcelona y en los superardenadores Mare Nostrum y Finisterrae de la Red Española de Supercomputación (RES).

Así pues, este trabajo se estructura en dos partes. En la primera (capítulos 2, 3 y 4) se explica la estructura y parametrización del código *Ludwig* así como el análisis de los resultados de las simulaciones realizadas. En la segunda parte se hace una descripción del *SABRA-model* generalizado y el correspondiente análisis de resultados (capítulo 5).

La estructura por capítulos es la siguiente:

- El primer capítulo define los conceptos básicos en el estudio de *active matter* y se centra en el marco teórico.
- En el Capítulo 2 explicamos la metodología numérica que utilizamos para simular el fluido que interactúa con las partículas, así como una descripción del modelo de partícula utilizado y sus mecanismos de movimiento autoconducido.

- El Capítulo 3 muestra algunos resultados sobre la orientación y desplazamiento de las partículas desde un punto de vista estadístico, estableciendo diferencias notables para distintas parametrizaciones en las simulaciones.
- En el Capítulo 4 estudiamos los espectros de energía y las distribuciones de velocidad para mejorar el conocimiento de la interacción entre escalas.
- Shell-model en general y *SabrActive-model* específicamente se describen en el Capítulo 5 y también explicamos el correspondiente análisis de los resultados de las simulaciones.
- Finalmente, se encuentran las conclusiones y perspectivas que nos permiten validar a partir de los resultados las ecuaciones propuestas como hipótesis de esta tesis.

Simulation log table

ϕ	$size$	b_1	b_2	β	$TSTEP$
0.12	128	0.01	0.01	1	1.2×10^6
0.12	128	0.01	-0.01	-1	4×10^5
0.12	128	0.05	0.01	0.2	4×10^5
0.12	128	0.05	-0.01	-0.2	4×10^5
0.12	128	0.1	0.01	0.1	4×10^5
0.12	128	0.1	-0.01	-0.1	4×10^5
0.12	128	0	0.01	$+\infty$	4×10^5
0.12	128	0	-0.01	$-\infty$	4×10^5
0.12	128	0.01	0.1	10	4×10^5
0.12	128	0.01	-0.1	-10	4×10^5
0.12	128	0.01	0.2	20	4×10^5
0.12	128	0.01	-0.2	-20	4×10^5
0.12	512	0.01	-0.05	-5	2×10^6
0.06	128	0.01	0.01	1	4×10^6
0.06	128	0.01	0.01	1	2×10^6
0.06	128	0.01	0.01	1	1.2×10^6
0.06	128	0.01	-0.01	-1	4×10^5
0.06	256	0.01	0.01	1	2×10^6
0.06	512	0.01	0.01	1	2×10^6
0.06	512	0.01	-0.05	-5	2×10^6
0.03	128	0.01	0.01	1	1.2×10^6
0.03	128	0.01	-0.01	-1	4×10^5
0.012	128	0.01	0.01	1	1.2×10^6
0.012	128	0.01	-0.01	-1	4×10^5
0.012	128	0.01	0.05	5	4×10^5
0.012	128	0.01	-0.05	-5	4×10^5
0.012	512	0.01	-0.05	-5	2×10^6

Publications

The work presented throughout this thesis will be published as the following articles. As of the date of presentation of this thesis (September 2023), both have been submitted to the review of the referees.

- ALARCÓN, F; GASCÓ. A; SCAGLIARINI, A; PAGONABARRAGA, A (2023) Flocking, macroscopic clusters and super-diffusion in 3D microswimmer suspensions

- GASCÓ. A; SCAGLIARINI, A; PAGONABARRAGA, A (2023) Three-dimensional active turbulence in microswimmer suspensions: simulations and modelling.

List of Figures

LIST OF FIGURES

References

[1] FRISH, U. (1995) Turbulence: The Legacy of A. N. Kolmogorov. UK: Cambridge University Press

[2] SÁNCHEZ, C; VALDÉS, C (2003) Kolmogorov: el zar del azar. España: Nivola libros y ediciones, SL

[3] VAN DYCKE, M. (1982) An album of fluid motion. USA: The Parabolic Press

[4] RICHARDSON, L (1920) The Supply energy from and to atmospheric eddies. Proceedings of the Royal Society of London. Series A, Containing Papers of a Mathematical and Physical Character, 97, Issue 686, 354-373

[5] TAYLOR, G.I. (1931) Effect of Variation in Density on the Stability of Superposed Streams of Fluid. Proceedings of the Royal Society of London. Series A, Containing Papers of a Mathematical and Physical Character, 132, Issue 820, 499-523

[6] CARDY, J; FALKOVICH, G; GAWEDZKI, K (2008) Non equilibrium statistical mechanics and turbulence. LONDON: Cambridge University Press

[7] AJINENKO, I and 36 OTHERS (1989) Intermittency patterns in collisions at 250 GeV. Physics letters B, 222, 306-310

[8] BOHR, T; JENSEN, M.H; PALADIN, G; VULPIANI, A (1998) Dynamical Systems Approach to Turbulence. UK: Cambridge University Press

[9] TOUIL,H; RICOT,D; LEVEQUE, E (2013) Direct and Large-Eddy Simulation of Turbulent Flows on Composite Multi-Resolution Grids by the Lattice Boltzmann Method. JOURNAL COMPUTATIONAL PHYSICS, 256, 220-233

[10] SAGAUT,P; MALASPINAS,O (2014) Consistent subgrid scale modelling for lattice Boltzmann methods. Journal of Fluid Mechanics , 700, pp. 514 - 542

[11] GIOMI, L. (2015) Geometry and topology of turbulence in active nematics. Physical Review X, 5, Issue 3, 031003

[12] BRATANOV, V;JENKO, F; FREY, E (2015) New class of turbulence in active fluids. Proceedings of the National Academy of Sciences, 112, 15048-53

[13] THAMPI, S.P; YEOMANS, J.M. (2016) Active turbulence in active nematics. The European Physical Journal Special Topics, 225, 4, 651-662

[14] MARCHETTI, M.C; JOANNY, J.F; RAMASWAMY, S; LIVERPOOL, T.B; PROST, J; RAO, M; SIMHA, R.A. (2013) Hidrodynamics of soft active matter. Reviews of modern physics, 85,

[15] THAMPI,S.P; DOOSTMOHAMMADI, A; SHENDRUCK, T.N; GOLESTANIAN, R; YEOMANS, J.M (2016) Active micromachines: microfluids powered by mesoscale turbulence. Science Advances 2,e1501854

[16] WENSINK H.H; DUNKEL, J; HEIDENREICH, S; DRESCHER, K; GOLDSTEIN, R.E; LÖWEN, H; YEOMANS, J.M. (2012) Meso-scale turbulence in living fluids. Proceedings of the National Academy of Sciences of the United States of America, 109(36), 14308-13

[17] QIU, X; DING, L; HUANG, Y; CHEN, M; LU, Z; LIU, Y; ZHOU,Q (2016) Intermittency measurement in two-dimensional bacterial turbulence. Physical review E, 93, 062226

[18] HEMINGWAY, E.J; MAITRA, A; MARCHETTI, M.C; RAMASWAMY, S; FIELDING, S.M; CATES, M.E. (2015) Active viscoelastic matter: from bacterial drag reduction to turbulent solids. Physical review letters, 114, 098302

[19] CREPPY, A; PRAUD, O; DRUART, X; KOHNKE, P; PLOURABOUÉ,F. (2015) Turbulence of swarming sperm. Physical review E, 92, issue 3,032722

[20] HEMINGWAY, E.J; CATES, M.E; FIELDING, S.M. (2016) Viscoelastic and elastomeric active matter: linear instability and nonlinear dynamics. Physical review E, 93, 032702

[21] DE GENNES, P.G.; PROST, J. (1974) The physics of Liquid Crystals. UK: Oxford Science Publications

[22] GLEDZER, E.B (1977) System of hidrodynamic type admitting two quadratic integrals of motion Sov. Phys. Dokl 18, 216

[23] YAMADA, M; OHKITANI, K. (1987) Lyapunov spectrum of a model of two-dimensional turbulence. Physical Review Letters, 60, 11, 983-986

[24] YAMADA, M; OHKITANI, K. (1988) The inertial subrange and non-positive Lyapunov exponents in fully-developed turbulence. Progress Theorical Physics, 79, 1265-1268

[25] YAMADA, M; SAIKI,Y (2007) Chaotic properties of fuylly developed model turbulence. Non linear Processes in geophysics, 14, 631-647

[26] WALEFFE,F. (1992) The nature of triad interactions in homogeneous turbulence. Physics of Fluids A, 4, 350-363

[27] SAHOO,G; ALEXAKIS, A; BIFERALE, L. (2017) Discontinuous transition from direct to inverse cascade in 3-dimensional turbulence. Physical Review Letters, 118, 164501

[28] BIFERALE, L (1995) Helical Shell Models for 3-dimensional Turbulence. Physical Review E, 53(4), 3541-3550

[29] RATHMANN, N.M; DITLEVSEN, D (2016) The role of helicity in triad interactions in 3D turbulence investigated in a new shelll model. Physical Review E, 94, 033115

[30] BUZZICOTTI, M; BHATNAGAR, A: BIFERALE, L; LANOTTE, A; SANKAR, S. (2016) Lagrangian statics for Navier-Stokes turbulence under Fourier-mode reduction: fractal and homogeneous decimations. New Journal of Physics, 18, 113047

[31] DE PIETRO, M; BIFERALE;L; MAILYBAEV, A. (2015) Inverse energy cascade in non local helical shell models of turbulence. Physical Review E, 92, 043021

[32] BIFERALE, L; MUSACCHIO, S; TOSCHI, F. (2012) Inverse energy cascade in 3-dimensional isotropic turbulence. Physical Review Letters, 108, 164501

[33] DITLEVSEN, P.D. (2000) Symmetries, invariants and cascades in a shell model of turbulence. Physical Review E, 62, 484

[34] L'VOV, V; PODIVILOV, A; PROCACCIA, I; VANDEMBROUCQ, D. (1998) Improved shell model of turbulence. Physical Review E, 58, 1811

[35] SCAGLIARINI,A; PAGONABARRAGA, I. Notes of the characterization of turbulent states in bacterial suspensions *(pending publication)*

[36] BIFERALE, L; LAMBERT, A; LIMA, R; PALADIN, G. (1994) Transition to chaos in a shell model of turbulence. Physica D: Nonlinear Phenomena, Volume 80, Issue 1-2, 105-119

[37] RITHWIK, T; SMRIDDHI, S. (2017) Revisiting the SABRA model: statics and dynamics. Europhysics Letters, 120, 3, 34002

[38] ANGHELUTA, L; BENZI, R; BIFERALE, L; PROCACCIA, I. (2006) On the anomalous scaling exponents in non linear models of turbulence. Physical Review Letters, 97, 16, 160601

[39] BENZI, R; CHING, E; HORESH, N; PROCACCIA, I. (2004) Theory of concentration dependence in drag reduction by polymers and maximum drag reduction asymptote. Phys. Rev. Lett. 92, issue 7, 078302

[40] DE PIETRO, M; BIFERALE;L; MAILYBAEV, A. (2015) Inverse energy cascade in non local helical shell models of turbulence. Phys. Rev. E, 92, issue 4, 043021

[41] DESPLAT, J.G; PAGONABARRAGA, I; BLADON, P (2001) LUDWIG: A parallel lattice-Boltzmann code for complex fluids. Comput. Phys. Comms., 134, 273

[42] CARENZA, L.N. ; BIFERALE, L. ; GONNELLA, G. (2020) Multiscale control of "active emulsion" dynamics, Fis. Rev. Fluid 5, 011302(R) American Physical Society.

[43] SAINTILLAN, D. ; SHELLEY, M.J. (2012)Emergence of coherent structures and large-scale flows in mobile suspensions J. R. Soc. Interfície **69**, 571-585 Royal Society.

[44] BÁRDFALVY, D. ; NORDANGER, H. ; NARDINI, C. ; MOROZOV, A. ; STENHAMMAR, J. (2019) Boltzmann simulations of jealousy solved by 'three-dimensional active turbulence particles, soft matter' 15, 7747-7756, Royal Society of Chemistry.

[45] ALARCÓN, F; PAGONABARRAGA,I. (2013) Spontaneous aggregation and global polar arrangement in squimer suspensions , Journal of molecular liquids 185, 56

[46] ADITI SIMHA, R; RAMASWAMY, S. (2002)Hydrodynamic fluctuations and instabilities in ordered suspensions of self-propelled particles Phys. Rev. Lett. 89, 058101.

[47] HATWALNE, Y; RAMASWAMY, S; RAO, M; ADITI SIMHA, R (2004)Rheology of active-particle suspensions Phys. Rev. Lett. 92, 118101

[48] SAINTILLAN, D. ; SHELLEY, M.J.(2008) Instabilities, pattern formation, and mixing in active suspensions Phys. Rev. Lett. 100, 178103.

[49] SAINTILLAN, D. ; SHELLEY, M.J.(2008) Instabilities and pattern formation in active particle suspensions: kinetic theory and continuum simulations Phys. Fluids 20, 123304.

[50] BASKARAN, Q; MARCHETTI, M. (2009) Statistical mechanics and hydrodynamics of bacterial suspensions. Proc. Natl. Acad. Sci. USA 106, 15567.

[51] PISMEN, LEN (2021) Active Matter whitin and around us. Switzerland: Springer

[52] LIGHTHILL M. J. (1952) On the squirming motion of nearly spherical deformable bodies through liquids at very small reynolds numbers Communications on Pure and Applied Mathematics, 5, 109–118

[53] BLAKE, J. R. (1971) A spherical envelope approach to ciliary propulsion. Journal of Fluid Mechanics, 46, 199–208

[54] ISIKAWA, T. (2009) Suspension biomechanics of swimming microbes. Journal of The Royal Society Interface, 6, (39), 815–834

[55] LAUGA, E; POWERS T. R.(2009) The hydrodynamics of swimming microorganisms. Reports on Progress in Physics, 72, (9), 096601

[56] PAK, O; LAUGA E. (2014) Generalized squirming motion of a spher. Journal of Engineering Mathematics, 88, (1), 1–28

[57] Ludwig User Manual (2017)

[58] CHEN, S; DOOLEN G.D. (1998) Lattice Boltzmann Method for fluid flows. Annu. Rev. Fluid Mech., 30, (1), 329–364

[59] FENG, Y.T; KOOK, N.H; OWEN, D.R.J (2007) Coupled lattice Boltzmann method and discrete element modeling of particle transport in turbulent fluid flows: Computational issues. International Journal for Numerical Methods in Engineering, 72, 1111-1134

[60] LADD A. (1994) Numerical simulations of fluid particulate suspensions via a discretized Boltzmann equation (Parts I-II). Journal of Fluid Mechanics, 271, 285–339

[61] NOBLE D, TORCZYNSKI J.(1998) A lattice Boltzmann method for partially saturated cells. International Journal of Modern Physics C, 9, 1189–1201

[62] ISHIKAWA, T; PEDLEY, T. (2014) Dispersion of model microorganisms swimming in a nonuniform suspension Phys. Rev. E, 90, 03308

[63] ISHIKAWA, T; PEDLEY, T. (2007) Diffusion of swimming model micro-organisms in a semi-dilute suspension Journal of Fluid Mechanics, 588, 437

[64] ALARCÓN, F.; SCLAGLIARINI, A.; GASCÓ, A.; PAGONABARRAGA, I. (2023) Macroscopic clusters and super-diffusion in 3D-microsimmer suspensions. *(pending publication)*

[65] SCLAGLIARINI, A.; GASCÓ, A.; PAGONABARRAGA, I. (2023) Three-dimensional active turbulence in microswimmer suspensions: simulations and modelling *(pending publication)*

[66] EVANS, A. A., ISHIKAWA, T., YAMAGUCHI, T., LAUGA, E. (2011). Orientational order in concentrated suspensions of spherical microswimmers. Physics of Fluids, 23(11).